Kübra FEVZİOĞLU

DENSITY FUNCTIONAL THEORY STUDIES ON STRUCTURAL AND SPECTRAL CHARACTERISTICS OF *o*-ANISIDINE

M.S.
2015

FATİH UNIVERSITY

The Graduate School of Sciences and Engineering

Master of Science in
Physics

DENSITY FUNCTIONAL THEORY STUDIES ON STRUCTURAL AND SPECTRAL CHARACTERISTICS OF *o*-ANISIDINE

by

Kübra FEVZİOĞLU

June 2015

DENSITY FUNCTIONAL THEORY STUDIES ON STRUCTURAL AND SPECTRAL CHARACTERISTICS OF *o*-ANISIDINE

by

Kübra FEVZİOĞLU

A thesis submitted to

the Graduate School of Sciences and Engineering

of

Fatih University

in partial fulfillment of the requirements for the degree of

Master of Science

in

Physics

June 2015
Istanbul, Turkey

APPROVAL PAGE

This is to certify that I have read this thesis written by Kübra FEVZİOĞLU and that in my opinion it is fully adequate, in scope and quality, as a thesis for the degree of Master of Science in Physics.

_____
Assoc. Prof. Ahmet ALTUN
Supervisor

_____
Prof. Naz Mohammed ATABAY
Co-Supervisor

I certify that this thesis satisfies all the requirements as a thesis for the degree of Master of Science in Physics.

_____
Prof. Mustafa KUMRU
Head of Department

Examining Committee Members

Assoc. Prof. Ahmet ALTUN _____

Prof. Mustafa KUMRU _____

Assoc. Prof. Mehmet KARABACAK _____

It is approved that this thesis has been written in compliance with the formatting rules laid down by the Graduate School of Sciences and Engineering.

_____
Prof. Nurullah ARSLAN
Director

June 2015

DENSITY FUNCTIONAL THEORY STUDIES ON STRUCTURAL AND SPECTRAL CHARACTERISTICS OF *o*-ANISIDINE

Kübra FEVZİOĞLU

M.S. Thesis – Physics
July 2015

Thesis Supervisor: Assoc. Prof. Ahmet ALTUN

Co-Supervisor: Prof. Naz Mohammed ATABAY

ABSTRACT

The molecular structures, vibrational spectra (IR and Raman), UV-Vis electronic absorption spectra, and NMR spectra (^{13}C and ^{1}H) of *o*-anisidine have been investigated in terms of density functional theory by using B3LYP as a density functional and 6-311++G** as a basis set. Two stable and virtually degenerate conformers arising from non-planarity of the amino group have been located at the room temperature for *o*-anisidine. The calculated spectroscopic characteristics of these conformers have been found almost identical. All normal modes of *o*-anisidine have been assigned expressing percent contributions of the internal motions. All main transitions in the electronic absorption spectrum of *o*-anisidine have been assigned in terms of the present calculations. Solution has been shown to affect the unoccupied orbitals of *o*-anisidine drastically, which shift all electronic absorption bands to longer wavelengths. Solution increases ionization potential of *o*-anisidine but decreases its electron affinity. The present chemical shift calculations allow certain assignments of the experimental ^{13}C and ^{1}H NMR signals of *o*-anisidine. The frontier molecular orbital, molecular electrostatic potential map, and atomic charge (Mulliken, ESP, and NBO) analyses have been shown useful in estimating both global and atom-in-molecule characteristics of *o*-anisidine. The high correlations between experimental and the present computational spectral data allow one to follow the computational route presented in this study for studying spectroscopic characteristics of analogous compounds.

Keywords: *o*-Anisidine, Density Functional Theory (DFT), Infrared, Raman, Normal mode, UV-Vis, NMR

o-ANİSİDİN MOLEKÜLÜNÜN YAPISAL VE SPEKTRAL KARAKTERİSTİKLERİNİN YOĞUNLUK FONKSİYONEL TEORİ İLE İNCELENMESİ

Kübra FEVZİOĞLU

Yüksek Lisans Tezi – Physics
February 2014

Tez Danışmanı: Doç. Dr. Ahmet ALTUN

Eş Danışman: Prof. Dr. Naz Mohammed ATABAY

ÖZ

o-Anisidin molekülünün geometrik yapısı, titreşim (IR ve Raman), UV-Vis elektronik soğurma ve NMR (^{13}C ve ^{1}H) spektrumları yoğunluk fonksiyonel teori ile B3LYP yoğunluk fonksiyoneli ve 6-311++G** temel kümesi kullanılarak elde edildi. *o*-Anisidinin oda sıcaklığında amino grubunun düzlemsel olmamasından kaynaklanan aynı enerjetik kararlığa sahip iki konformeri bulundu. *o*-Anisidinin bütün normal modları iç hareketlerin yüzdelik katkıları verilerek tanımlandı. *o*-Anisidinin elektronik soğurma spektrumundaki bütün ana geçişler hesap sonuçlarına dayalı olarak tanımlandı. Çözeltinin özellikle dolu olmayan moleküler orbitalleri etkileyerek bütün elektronik soğurma bandlarını uzun dalgaboylarına kaydırdığı bulundu. Çözeltinin ayrıca *o*-anisidinin iyonlaşma potansiyelini arttırırken elektron ilgisini azalttığı bulundu. *o*-Anisidinin kimyasal kayma hesaplamaları deneysel ^{13}C ve ^{1}H NMR sinyallerinin kesin tanımına yol açmıştır. Öncül moleküler orbital, moleküler elektrostatik potansiyel haritası, ve atomik yük (Mulliken, ESP ve NBO) analizleri *o*-anisidinin hem global hemde atomik seviyedeki özelliklerinin ortaya konulmasını sağlamıştır. *o*-Anisidinin deneysel ve teorik spektral verileri arasındaki yüksek korelasyon bu çalışmada takip edilen hesap protokollerinin benzer moleküllerin spektroskopik karakteristiklerinin bulunmasında kullanılabileceğini göstermektedir.

Anahtar Kelimeler: *o*-Anisidin, Yoğunluk fonksiyonel teori, İnfrared, Raman, Normal mod, UV-Vis, NMR

To My Family

ACKNOWLEDGEMENT

I express sincere appreciation to Assoc. Prof. Ahmet ALTUN for his guidance and insight throughout the research.

Thanks go to the other faculty members, Prof. Mustafa KUMRU, Prof. Sadık GÜNER, Prof. Serkan ÇALIŞKAN, Assoc. Prof. Levent SARI and Dr. Tayyibe BARDAKÇI for their valuable suggestions and comments.

I am thankful to all my friends for their motivation and support especially Sinem ESİR, Esra YAZICI, Aseel ALMARMORI, Haidar Mas'ud ALFANDA, Onur DURUCAN, Gülsüm YILDIZHAN, Esra KOÇ, Merve TAŞ, Zeynep Rüya DEVELİ, Esra OKUMUŞ and Hacer BAYÇÖL.

I express my thanks and appreciation to my family especially my sister Merve FEVZİOĞLU for their understanding, motivation and patience. Lastly, but in no sense the least, I am thankful to all faculty members and friends who made my stay at the university a memorable and valuable experience.

TABLE OF CONTENTS

LIST OF TABLES

TABLE

LIST OF FIGURES

FIGURE

LIST OF SYMBOLS AND ABBREVIATIONS

SYMBOL/ABBREVIATION

2MTA	2-(Methylthio)aniline
B3LYP	Becke's three parameter Exchange Functional combined with Lee-Yang-Parr Correlation Functional
c	Speed of Light
DFT	Density Functional Theory
ESP	Electrostatic Potential
GGA	Generalized Gradient Approximation
GIAO	Gauge Including Atomic Orbital
h	Planck's Constant
HOMO	Highest Occupied Molecular Orbital
IR	Infrared
k	Boltzmann's Constant
KS	Kohn-Sham
LDA	Local Density Approximation
LUMO	Lowest Unoccupied Molecular Orbital
MAE	Mean Absolute Error
MESP	Molecular Electrostatic Potential
NBO	Natural Bond Orbital
NMR	Nuclear Magnetic Resonance
PCM	Polarizable Continuum Model
PED	Potential Energy Distribution
S	Standard Error
TD-DFT	Time-Dependent Density Functional Theory
TMS	Tetramethylsilane
UV-Vis	Ultraviolet–Visible
V_{XC}	Exchange-Correlation Potential

XC	Exchange-Correlation
α	Polarizability
β	In-Plane Deformation
γ	Out of Plane Deformation
δ	Chemical Shift
ε_i	Kohn-Sham Orbital Energies
μ_0	Dipole Moment of the System in Equilibrium
ν	Stretching
$\rho(r)$	Electron Density

CHAPTER 1

INTRODUCTION

Aniline is an organic compound that has a chemical formula of C_6H_7N. It is also known as aminobenzene, phenylamine, and benzenamine. It is the simplest amine with an aromatic ring. Aromatic amines are very important in biological as well as materials science. Aniline and its derivatives are of great industrial importance, particularly in the pharmaceutical and several other chemical industries. Investigations on the structures and vibrations of aniline derivatives in both ground and excited states attract considerable attention since they provide invaluable information about the nature of their molecular properties and chemical reactions that they undergo [1-10].

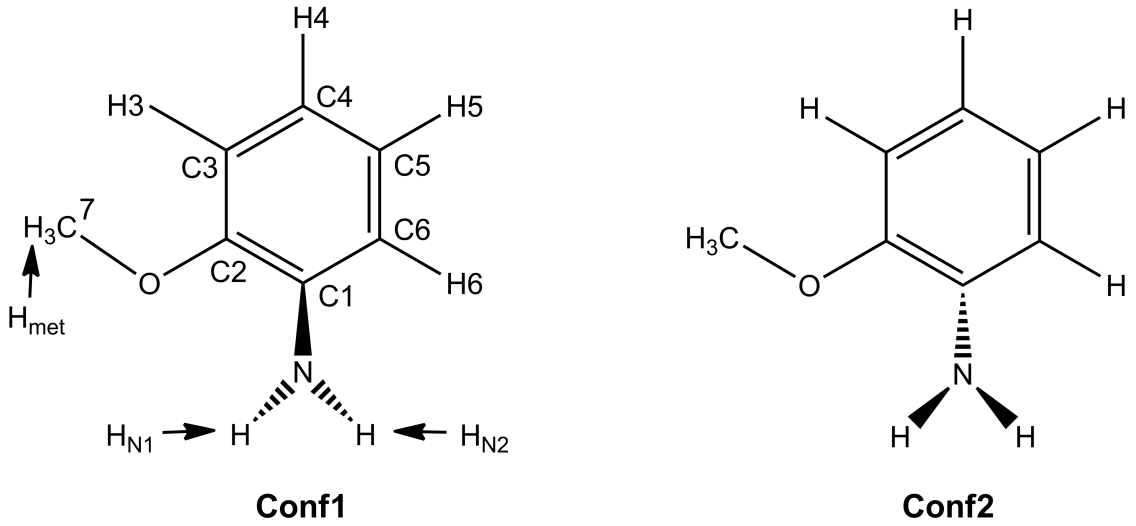

Figure 1.1 Two possible conformations of *o*-anisidine.

o-Anisidine, known also as 2-methoxyaniline, is an $–OCH_3$ derivative of aniline at the *ortho* position (see Figure 1.1). Although many pigments and dyes that are widely used in printing, and paper and textile dyeing are manufactured using *o*-anisidine, it is an industrial and environmental pollutant causing tumors of the urinary bladder in rats and mice, with potent carcinogenicity to human. In addition to its release from textiles and leather products, cigarette smoke releases also this carcinogen. *o*-Anisidine exhibits many other toxic effects, including hematological changes, anemia, and nephrotoxicity. It is also mutagenic to *Salmonella*. Hepatic microsomal cytochrome P450 enzymes in human, rat, and rabbit play an important role in the detoxication of this carcinogen [11-14].

Density functional theory (DFT) calculations with hybrid functionals like B3LYP are known to give quite accurate results for the geometrical and spectral characteristics of molecular systems. In this thesis, after a brief description of DFT and the fundamentals of vibrational spectra, we investigate structural and spectral characteristics of *o*-anisidine with the B3LYP functional. The theoretically investigated molecular characteristics include conformational stabilities, key geometry parameters, charge distributions, vibrational spectra (both IR and Raman), electronic absorption spectra, and ^{1}H and ^{13}C nuclear magnetic resonance spectra.

CHAPTER 2

THEORY

2.1 DENSITY FUNCTIONAL THEORY

Density functional theory (DFT) is a quantum mechanical method and determines many-body interacting system for the ground state properties via electronic density rather than many-body wave function. It is based on Hohenberg-Kohn theorem which expresses that all electronic properties of both ground and excited states can be determined by electron density $\rho(\vec{r})$ at any position $\vec{r}$ in the space. Unfortunately, the Hohenberg-Kohn theorem does not describe how to calculate the electron density. The way of obtaining the electron density is given by Kohn and Sham formalism [15-18]. The ground state electron density $\rho(\vec{r})$ can be written in terms of the one-electron spatial orbitals $\psi_i(\vec{r})$ called Kohn-Sham (KS) orbitals as

$$\rho(\vec{r}) = \sum_{i=1}^{n} \left|\psi_i(\vec{r})\right|^2 \tag{2.1}$$

This allows reducing many-electron equation to one-electron equation as

$$\left\{-\frac{\hbar^2}{2m_e}\nabla_1^2 - \frac{e^2}{4\pi\varepsilon_0}\sum_{S=1}^{N}\frac{Z_S}{r_{S1}} + \frac{e^2}{4\pi\varepsilon_0}\int\frac{\rho(\vec{r}_2)}{r_{12}}d\vec{r}_2 + V_{XC}(\vec{r}_1)\right\}\psi_i(\vec{r}_1) = \varepsilon_i\psi_i(\vec{r}_1) \tag{2.2}$$

where ε_i corresponds to the KS orbital energy, the first term in Eq (2.2) is the kinetic energy, the second term is the electron-nucleus attraction with the sum over all N nuclei with the atomic number Z, the third term is the electron-electron Coulomb interaction,

and the last term V_{XC} is the exchange-correlation (XC) potential, which is the functional derivative of the exchange-correlation energy [19-21].

Although DFT is exact, the functional form of the XC energy is not known. Therefore, many approximations, like Local density approximation (LDA), Generalized gradient approximation (GGA), and hybrid density functional, have been proposed for calculating the XC energy. For molecular systems, a remarkable accuracy has been achieved by hybrid density functionals. One of the most widely used hybrid density functionals is Becke's three-parameter exchange functional combined with Lee-Yang-Parr correlation functional known as B3LYP.

The Kohn-Sham equations are in general solved self-consistently. One starts with a set of trial KS orbitals of $\psi_i(\vec{r})$ that yield electron density according to Eq.(2.1). With the resulting electron density, XC potential is calculated. These are inserted into Eq. (2.2) for obtaining the $\psi_i(\vec{r})$ functions. From these new one-electron functions, an improved electron density is calculated through Eq. (2.1). This procedure is repeated until the electron density and XC energy are converged within some certain tolerances [22, 23]. The KS orbitals can be computed numerically or they can be expressed in term of a set of basis functions at each iteration.

2.2 VIBRATIONAL SPECTROSCOPY

2.2.1 Fundamentals of Vibrational Spectra

The atoms of a molecule are in motion due to translational, rotational, and vibrational degrees of freedom. As each atom is defined with 3 degrees of freedom (x, y, and z), a molecule with N atoms has 3N degrees of freedom [24]. Three of those correspond to translation of the molecule while two and three of them are for rotational motion for linear and nonlinear molecules, respectively. The remaining 3N-5 or 3N-6 degrees of freedom are for the vibrations of linear and non-linear molecules, respectively.

When a molecule is excited vibrationally, its potential energy depends on the displacements of all the atoms from their equilibrium positions and can be written as

$$U = U(0) + \sum_i \left(\frac{\partial U}{\partial x_i} \right)_0 x_i + \frac{1}{2} \sum_{i,j} \left(\frac{\partial^2 U}{\partial x_i \partial x_j} \right)_0 x_i x_j + ... \tag{2.3}$$

Here the sum is over all the displacements. The zero subscript represents expansion around equilibrium bond lengths. Since the potential curve has a minimum at the equilibrium, the first derivatives are all zero. The change in potential energy for the small displacements from equilibrium is thus

$$U = \frac{1}{2} \sum_{i,j} k_{ij} x_i x_j ; \qquad k_{ij} = \left(\frac{\partial^2 U}{\partial x_i \partial x_j} \right)_0 \tag{2.4}$$

here k_{ij} is generalized force constant. These k_{ij} constants form the Hessian matrix. For local minimum this matrix has positive values, while it has negative values for saddle point. The mass-weighted coordinates are defined as

$$x_i = \frac{q_i}{\sqrt{m_i}} \tag{2.5}$$

here m_i is the mass of the displaced atom by x_i. In terms of the mass-weighted coordinates, potential energy and force constants can be expressed as

$$U = \frac{1}{2} \sum_{ij} K_{ij} q_i q_j \; ; \qquad K_{ij} = \frac{k_{ij}}{\sqrt{m_i m_j}} = \left(\frac{\partial^2 U}{\partial q_i \partial q_j} \right)_0 \tag{2.6}$$

while the total kinetic energy takes the form

$$T = \frac{1}{2} \sum_i m_i \dot{x}_i^2 = \frac{1}{2} \sum_i \dot{q}_i^2 \tag{2.7}$$

Therefore, the total energy becomes

$$E = \frac{1}{2} \sum_i \dot{q}_i^2 + \frac{1}{2} \sum_{ij} K_{ij} q_i q_j \tag{2.8}$$

For avoiding the difficulties in calculating the energies with Eq. (2.8) due to cross terms with different *i* and *j*, new coordinate sets expressed as the linear combinations of mass-weighted coordinates of the cross terms called normal coordinates *Q* can be defined, which allows writing the total energy without cross-term as

$$E = \frac{1}{2}\sum_i \dot{Q}_i^2 + \frac{1}{2}\sum_i \lambda_i Q_i^2 \tag{2.9}$$

Quantum mechanical solution of this harmonic potential yields

$$E_{v_i} = \left(v_i + \frac{1}{2} \right) \hbar \omega_i \; ; \qquad \omega_i = \sqrt{\lambda_i} \; ; \qquad v_i = 0,1,2,.... \tag{2.10}$$

These harmonic oscillator energy levels are equally spaced. However, for large displacements from equilibrium, the energetic separation between the adjacent levels becomes smaller while moving to the higher vibrational levels [25].

2.2.2 Infrared Spectroscopy

Infrared spectroscopy gives particular information about the structure of the molecules by absorption of the incident light in the infrared region of electromagnetic radiation via molecular vibration that cause a change in the dipole moment of the molecule [26, 27]. The process is controlled by the electrical dipole moment. The molecular dipole moment changing by normal coordinates around an equilibrium displacement can be written as

$$\mu = \mu_0 + \sum_i \left(\frac{\partial \mu}{\partial Q_i} \right)_0 Q_i + \frac{1}{2}\sum_i \left(\frac{\partial^2 \mu}{\partial Q_i^2} \right)_0 Q_i^2 + ... \tag{2.11}$$

where μ_0 is dipole moment of the system in equilibrium and termed as permanent dipole moment. For the small displacements from the equilibrium positions, the quadratic and higher order terms may be neglected. The electric dipole transition moment will then be

$$\langle 00...v_i'...0|\mu|00...v_i...0\rangle \approx \left(\frac{\partial \mu}{\partial Q_i}\right)_0 \langle v_i'|Q_i|v_i\rangle \tag{2.12}$$

Therefore, for a transition to be infrared active, the dipole moment must change along normal coordinates, i.e.

$$\left(\frac{\partial \mu}{\partial Q_i}\right)_0 \neq 0 \tag{2.13}$$

with the selection rule of $\Delta v=\pm 1$. However, for an anharmonic oscillator, there is no restriction on Δv. According to Boltzmann distribution, the population of $v=1$ state is just about one per cent of the ground state population ($v = 1$) at the room temperature. Therefore, the absorptions from $v = 1$ and higher levels do not contribute much to the spectrum. The main transitions from $v = 0$ to $v = 1$ are called fundamental transition.

2.2.3 Raman Spectroscopy

When a monochromatic light is sent onto a molecule, the photons are mostly scattered elastically having the same energy as the incident photons (Rayleigh scattering). A small fraction of photons (about 1 photon among ten millions photons) are scattered inelastically (Raman Scattering). In this case, if the incident photon energy excites the molecule vibrationally, this causes scattered photons that are diminished in energy by the amount of the vibrational transition energies (Stokes shift). If the scattered photon energy is higher than the incident one due to excitations from the excited state vibrational levels, the energy shift in such weak transitions is called anti-Stokes shift.

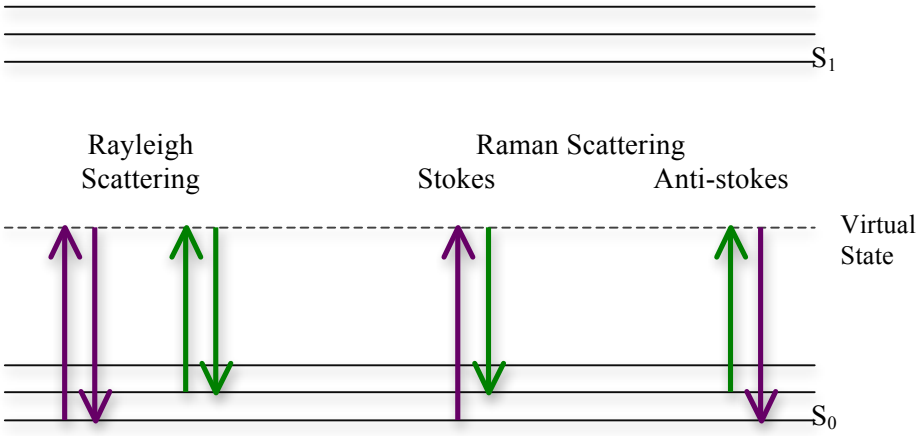

Figure 2.1 Scattering due to collision of photons and molecules.

An electromagnetic radiation with an electric field E perturbs charged particles of a molecule causing an induced moment μ.

$$\mu = \alpha E \tag{2.14}$$

where α is the polarizability. When a molecule undergoes some internal motion like vibration or rotation, the polarizability will be changed periodically. The molecular polarizability α can be expanded in terms of normal coordinates like Eq. (2.12). In this case, the transition dipole moment will be

$$\langle 00...v_i'...0|\mu|00...v_i...0\rangle \approx \left(\frac{\partial \alpha}{\partial Q_i}\right)_0 \langle v_i'|Q_i|v_i\rangle E \tag{2.15}$$

Therefore, a transition is Raman active if the polarizability change along the normal coordinates, i.e.

$$\left(\frac{\partial \alpha}{\partial Q_i}\right)_0 \neq 0 \tag{2.16}$$

with the selection rule of $\Delta v = \pm 1$ for harmonic oscillations. Again, for the anharmonic vibrations, there is no restriction on Δv.

2.3 SKELETAL AND GROUP VIBRATIONS

In some vibrational modes, almost all atoms undergo approximately the same displacement, called as skeletal vibration. However, in some modes, a small group of atoms move independently from the remainder, called as characteristic group vibrations. The skeletal vibrations mostly occur in the 1400-700 cm^{-1} range, which is sometimes called as fingerprint region because the vibrations in this region give distinctive information about the molecular structure. If any group in a molecule has heavier (Cl, Br, F, etc.) or lighter atoms (OH, NH, NH_2, CH_3, etc.), these groups have independent movement than the remainder of the molecule. The frequencies of such groups appear in the 3700-1500 cm^{-1} range, which is also called as functional group frequency region [28-32].

Vibration types can be mainly divided into two: stretching and deformation. The stretching vibration corresponds to bond length changing along the bond axis. The deformation vibration arises from the change in angles and can occur in several ways (scissoring, rocking, wagging, and twisting) as described in Figure 2.2.

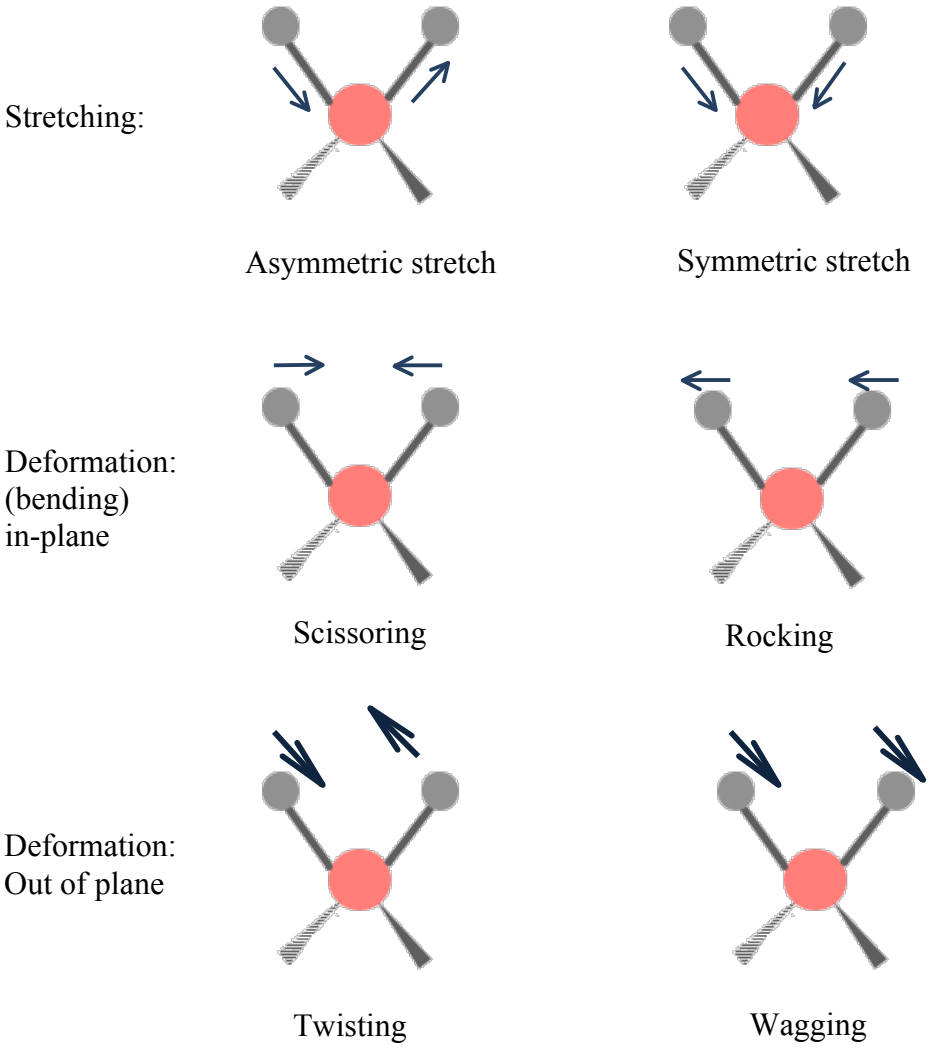

Figure 2.2 Vibration types of a CH_2 moiety.

CHAPTER 3

COMPUTATIONAL DETAILS

All quantum chemical calculations were performed by using Gaussian 03 (with Linda) program package on linux server cluster [33]. The geometrical structures of the two conformers of *o*-anisidine were optimized by using the hybrid B3LYP [34, 35] density functional and the split-valence 6-311++G** basis set [36-38]. The optimized structures were then used for spectral calculations. Unless stated otherwise, these spectral calculations were performed at the B3LYP/6-311++G** level.

Force fields of the compounds were calculated in the space of Cartesian coordinates by analytic differentiation. They were then transformed to internal coordinates for assigning normal modes in terms of internal motions (stretching ν; out-of-plane deformation γ; in-plane deformation β) with their percent contributions to the potential energy distribution (PED), which appeared consistent with the visualized atomic displacements by using the GaussView program [39].

B3LYP overestimates vibrational frequencies systematically as a result of the neglect of the effects of crystal packing and anharmonicity, and the incompleteness of basis set and dynamic correlation. Thus, the calculated frequencies are mostly scaled for relating the computed and experimental frequencies [40, 41]. We derived the scaling factors that are the correlation coefficients between the experimental and computed frequencies on benzene. The structure and vibrational spectra of benzene were determined again at the B3LYP/6-311++G** level. The scaling factors were found on benzene as 0.964 (R^2 = 0.64) for the frequencies above 2800 cm^{-1}, which correspond to

X–H stretchings (X = C, N, S, etc.), and as 0.981 (R^2 = 1.00) for the frequencies below 2800 cm^{-1}. The R^2 value of the correlation for the frequencies below 2800 cm^{-1} is 1.00,

which indicates that the found factor can be used in scaling computational frequencies of the related molecules. However, it is 0.64 for the frequencies above 3000 cm^{-1}, analogous to those obtained on other related compounds [42, 43]. Thus, the corresponding scaling factor for X-H stretchings may not be accurate enough for other compounds. The largeness of the deviations between the experimental and the scaled X-H stretching frequencies can be attributed to their strong anharmonicity and local environment differences, i.e., vacuum (calculation) vs. liquid (experiment). The simulated IR and Raman spectra of *o*-anisidine were obtained using computational frequencies scaled with these two factors (0.964 and 0.981) found on benzene (ν_i), computed IR intensities ($I_{IR,i}$), and Raman intensities ($I_{Ra,i}$) found through the computed Raman activity ($S_{Ra,i}$) using the following equation derived from Raman scattering theory for each mode *i* [44-49]:

$$I_{Ra,i} = \frac{f(\nu_0 - \nu_i)^4 S_{Ra,i}}{\nu_i \left[1 - \exp(-\frac{hc\nu_i}{kT})\right]} \tag{3.1}$$

where *h*, *c,* and *k* are Planck's constant, speed of light, and Boltzmann's constant; *f* is a factor that is common for all peak intensities; ν_0 is the excitation line of the laser used in Raman measurements in cm^{-1}. In the simulation of Raman spectrum, excitation line was taken that provided by a near infrared Nd:YAG air-cooled laser (1064 nm = 9398.5 cm^{-1}). IR and Raman spectra were simulated by using pure Lorentzian band shapes taking the full widths at the half-height (FWHH) as 10 cm^{-1}.

UV-Vis absorption spectra were calculated with time-dependent (TD)-DFT method utilizing B3LYP functional and 6-311++G** basis set in both gas phase and in ethanol but at gas-phase geometry. The UV-Vis spectra were simulated through the fifty-root TD-B3LYP vertical excitation energy calculations by summing Gaussian curves (FWHH = 10 nm) whose areas were fitted to the calculated oscillator strengths *f*. In the presence of ethanol, *o*-anisidine was placed in a cavity formed by a set of overlapping spheres in the frameworks of the solvent reaction field and then ethanol was treated implicitly by using polarizable continuum model (PCM) [50]. Frontier molecular orbital analyses were also performed to determine the nature of electronic

transitions. These analyses were also extended to the calculation of global molecular characteristics.

The B3LYP/6-311++G** geometries were subjected to the calculations of the isotropic NMR shielding constant with the Gauge Including Atomic Orbital (GIAO) method at again B3LYP/6-311++G** level. The isotropic ^{13}C and ^{1}H NMR chemical shifts were then obtained by subtracting the shielding constants of *o*-anisidine from those of tetramethylsilane (TMS) calculated at the same computational level (184.07 ppm for C and 31.97 ppm for H). The calculated chemical shifts are generally scaled for correlating them easier with experiments [51-56]. The necessity of the scaling arises from the fact that, although the calculations are carried out on single isolated molecules, the recorded NMR spectra are quite sensitive to the environment of the molecules (solvent used or packing in solid state). To assess the effect of geometry on the chemical shifts, these B3LYP/6-311++G** calculations were also performed at the B3LYP/6-31G* geometries. The calculated chemical shifts were expressed in this case relative to calculated TMS shielding constants at the same computational level (183.51 ppm for C and 31.89 ppm for H).

Charge distribution analyses were performed at the B3LYP/6-311++G** geometries with B3LYP using both 6-31G* and 6-311++G** basis sets. Mulliken, electrostatic potential (ESP), and the most sophisticated natural bond (NBO) schemes were all used in such charge calculations. Molecular electrostatic potential plots were also obtained for determining nucleophilic and electrophilic regions of *o*-anisidine.

CHAPTER 4

RESULTS AND DISCUSSIONS

4.1 MOLECULAR GEOMETRY

The molecular structures of *o*-anisidine were obtained with geometry optimizations at the B3LYP/6-31G* and B3LYP/6-311++G** levels. Two stable conformers of *o*-anisidine (Conf1 and Conf2; see Figures 1.1 and 4.1) were located arising from pyramidalized geometry of the amino group. The pyramidalized geometry of the amino group is due to a balance between opposing forces: the stability gained by the molecule as a whole arising from p–π conjugation of the nitrogen lone pair with the aromatic system versus that gained by the amine using highly directed sp^3 orbitals for bond formation [8, 9]. This asymmetric interaction between the amino group and the aromatic ring produces a small displacement of the nitrogen atom from the benzene plane.

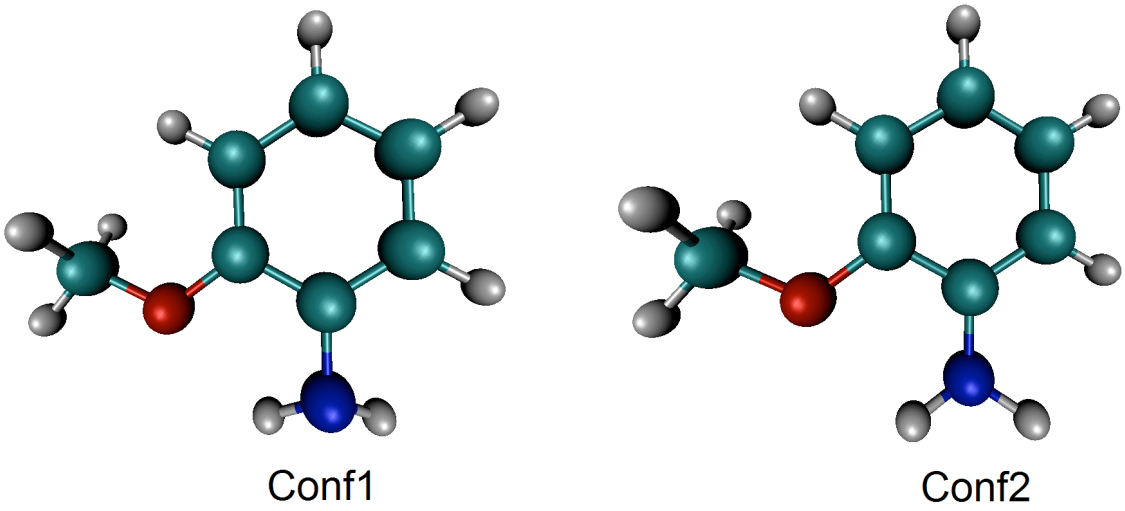

Figure 4.1 Two stable conformers of *o*-anisidine arising from pyramidalized geometry of the amino group.

Relative to the given orientation of the *o*-anisidine in Fig. 4.1, the C–N bond orients outside and inside of the page plane in Conf1 and Conf2, respectively. Therefore, amino hydrogen atoms orient inside and outside the page plane in Conf1 and Conf2, respectively. Only the rotamer due to methyl orientation with a dihedral angle C–O–C–H of ~180° is stable with vibrational frequencies that are all real. The other rotamers due to the methyl orientation have at least one imaginary frequency, and thus are not stable.

The Conf1 and Conf2 of *o*-anisidine are virtually degenerate, with slight preference to Conf2 (0.005 kcal/mol). The transition structure that connects Conf1 and Conf2 has planar amino group and lies just 0.74 kcal/mol above these conformers. These energetic data suggest that Conf1 and Conf2 of *o*-anisidine coexist at the room temperature as a mixture and are interconverted to each other fast.

The key geometry parameters (bond lengths, bond angles and torsional angles) of Conf1 and Conf2 obtained at the B3LYP/6-311++G** and B3LYP/6-31G* levels are as given in Table 4.1 using the atom labeling scheme shown on Figure 1.1. The Conf1 and Conf2 of *o*-anisidine do not contain any symmetry element other than identity. Thus, they belong to the C_1 point group.

The C–N bond of *o*-anisidine is out of the ring plane by 1.5° while the angle between the planes of the ring and amino group is calculated as 27° and 25° with 6-31G* and 6-311++G** basis sets, respectively (see the bottom of Table 4.1). These parameters about the structure of the amino group are very similar to those observed in aniline and its other derivatives [8, 9, 43]. The most significant geometry parameter differences between the 6-31G* and 6-311++G** geometries are due to amino group torsion angles and amount to 2°.

The C2–O bond of *o*-anisidine lies almost in the ring plane (see the bottom of Table 4.1). However, when the compound contains sulfur rather than oxygen [i.e., for 2-(methylthio)aniline], the C2–S bond is out of the ring plane by 1–2° [43]. The aromatic ring of *o*-anisidine is obviously distorted from a regular hexagon (Table 4.1), analogous to the observations on aniline and its other derivatives [8, 9, 43].

Table 4.1 Selected B3LYP/6-31G* and B3LYP/6-311++G** geometry parameters of *o*-anisidine.

Parameters	B3LYP/6-31G*		B3LYP/6-311++G**	
	Conf1	Conf2	Conf1	Conf2
Interatomic distance (Å)				
C1-C2	1.416	1.415	1.413	1.413
C2-C3	1.392	1.392	1.390	1.390
C3-C4	1.401	1.401	1.399	1.399
C4-C5	1.391	1.391	1.389	1.389
C5-C6	1.398	1.398	1.395	1.395
C1-C6	1.398	1.398	1.396	1.396
C2-O	1.376	1.376	1.374	1.374
C7-O	1.416	1.416	1.420	1.420
C1-N	1.397	1.397	1.394	1.394
N-H1	1.012	1.012	1.010	1.010
N-H2	1.012	1.012	1.009	1.009
C-H (ring) [a]	1.086	1.086	1.084	1.084
C-H (meth.) [a]	1.096	1.096	1.093	1.093
Bond angle (degree)				
C1-C2-C3	120.6	120.6	120.6	120.6
C2-C3-C4	120.1	120.1	120.2	120.2
C3-C4-C5	119.8	119.8	119.7	119.7
C4-C5-C6	120.1	120.1	120.1	120.1
C5-C6-C1	121.0	121.0	121.1	121.1
C6-C1-C2	118.3	118.3	118.3	118.3
N-C1-C2	119.2	119.2	119.3	119.3
N-C1-C6	122.4	122.4	122.3	122.4
C1-N-H_{N1}	113.5	113.5	114.7	114.7
C1-N-H_{N2}	114.5	114.5	115.7	115.7
H-N-H	112.3	112.3	113.5	113.5
H_{met}-C-H_{met} [a]	109.3	109.3	109.4	109.4
C2-O-C7	118.1	118.1	118.5	118.5
C1-C2-O	114.2	114.2	114.4	114.4
C3-C2-O	125.1	125.1	125.0	125.0
Torsional angle (degree)				
H_{N2}-N-C1-C2	153.0	-153.0	154.9	-155.3
H_{N1}-N-C1-C2	22.3	-22.3	19.9	-20.1
H_{N2}-N-C1-C6	-29.6	29.6	-27.7	27.4
H_{N1}-N-C1-C6	-160.4	160.4	-162.8	162.6
O-C2-C3-C4	-179.3	179.3	179.3	179.4
C6-C1-C2-O	179.1	-179.1	179.2	-179.3
C1-C2-O-C7	-179.4	179.5	-179.9	-179.8
C3-C2-O-C7	-0.005	0.049	-0.4	0.6
N-C1-H_{N1}-H_{N2}	-27.1	27.0	-24.7	24.6
C1-C6-C2-N	1.5	-1.5	1.5	-1.5
C2-C1-C3-O	-0.3	0.3	-0.3	0.2

[a] Averaged values

4.2 VIBRATIONAL SPECTRA

Several experimental IR and Raman spectra of the liquid *o*-anisidine recorded under different experimental settings were taken from spectral databases (gas phase IR [57]; IR in CCl_4 [58]; liquid film IR [58]; Raman in a Pyrex tube [59]) and shown on Figs. 4.2 and 4.3 together with the calculated IR and Raman spectra plotted using the scaled frequencies. The experimental and calculated (Conf1 and Conf2) vibrational characteristics of *o*-anisidine (frequencies, Raman scattering activities, IR/Raman intensities, assignments of the modes in terms of the percent PED of internal coordinates, and the correlation of the *o*-anisidine modes with benzene modes) are as given in Tables 4.2 and 4.3. As apparent from Figures 4.2 and 4.3, the vibrational spectra of Conf1 and Conf2 of *o*-anisidine are almost indistinguishable. Therefore, in the following, the Conf1 and Conf2 conformers will not be discussed separately.

Even after scaling, the calculated frequencies above 2800 cm^{-1} deviate significantly from the experimental frequencies. When compared with the gas-phase IR spectrum, standard error *S* and mean absolute error *MAE* in the scaled frequencies are 45 and 30 cm^{-1}, respectively. The *S* and *MAE* are 54 and 33 cm^{-1} compared with the liquid film IR spectrum. The R^2 value of the correlations in this range is 1.0. Therefore, the largeness of the error in the scaled frequencies does not arise from the use of scaling factor derived on benzene. The differences in the experimental frequencies of this range are mainly due to NH stretchings that are expected to be strongly environment-dependent and anharmonic. The calculated frequencies of the NH stretchings agree better with the gas-phase experimental IR frequencies than those observed in the other experimental settings since the calculations are also performed in the gas phase.

The modes with frequencies below 2800 cm^{-1} are not much affected from the experimental settings. Their frequencies are almost the same in the presently available experimental spectra. The S and *MAE* for the calculated frequencies of this range after scaling are just 9 and 6 cm^{-1}, respectively. Therefore, the scaling factor of the frequencies of this range derived on benzene is transferrable to other related molecules.

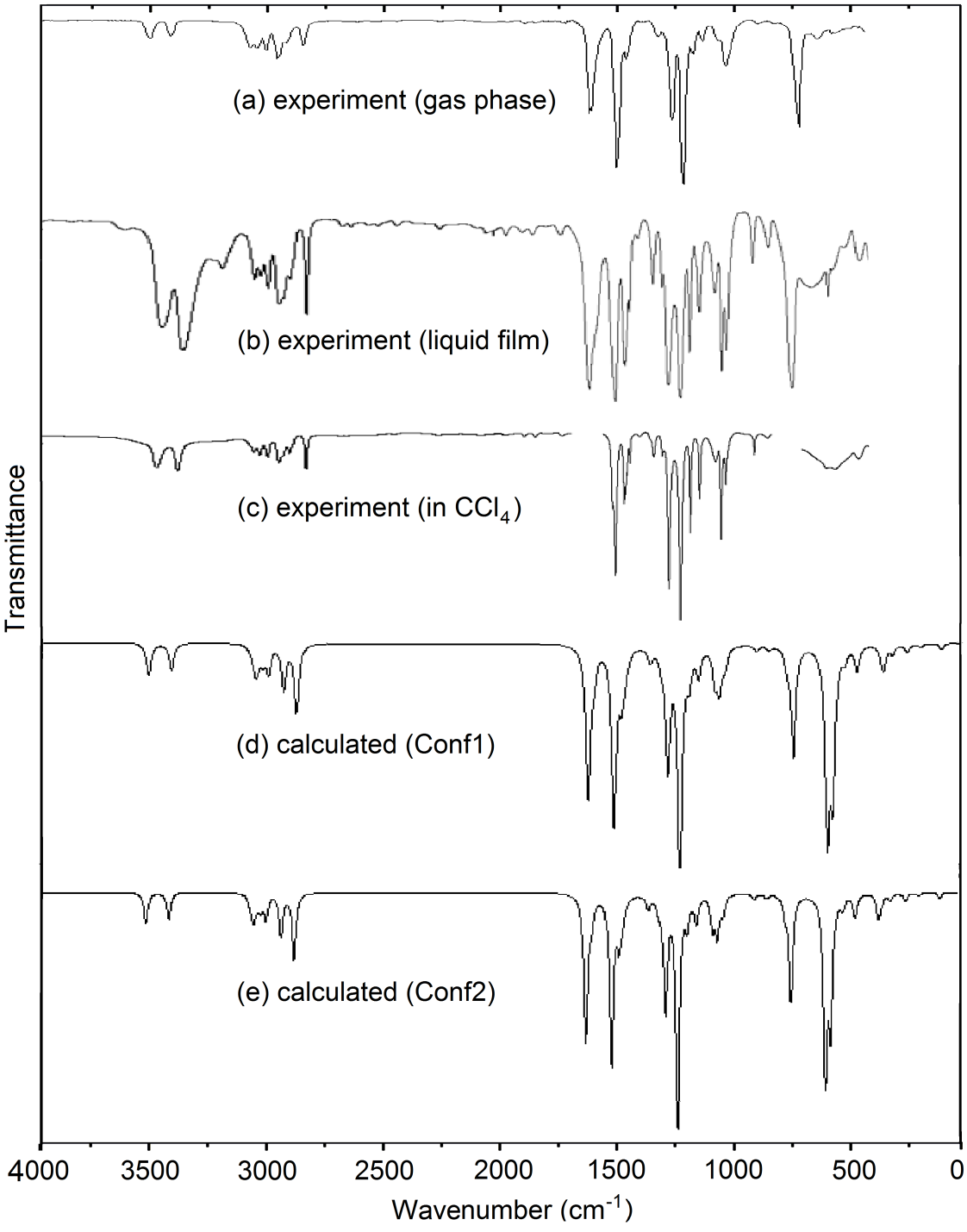

Figure 4.2 Experimental and simulated IR spectra of *o*-anisidine.

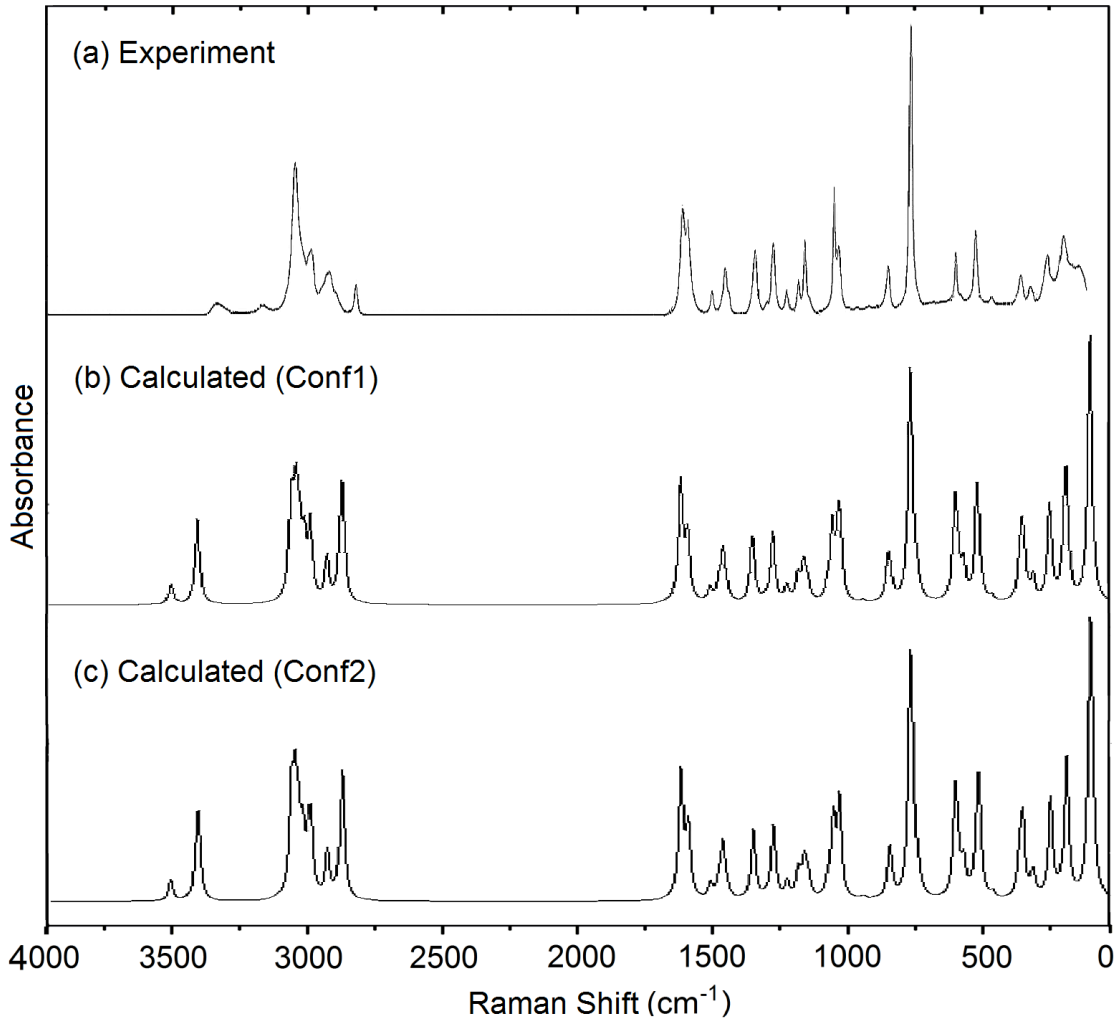

Figure 4.3 Experimental and simulated Raman spectra of *o*-anisidine.

Table 4.2 Calculated B3LYP/6-311++G** vibrational frequencies (in cm^{-1}), IR intensities, Raman scattering activities, Raman intensities, and normal mode descriptions for Conf1 of *o*-anisidine together with the experimental vibrational spectral characteristics of *o*-anisidine.

No[a]		Experimental[b]								Calculated					PED (%)
		IR (gas phase)[c]		IR (liquid film)[d]		IR (in CCl_4)[d]		Raman[e]		Unscaled	Scaled	I_{IR}	S_{IR}	I_{Ra}	
1		3501	m	3460	s	3487	m			3674	3541	27.36	47.99	15.95	100 νNH_2(asym.)
2		3412	m	3370	s	3396	m	3355	w	3570	3442	22.97	189.41	69.28	100 νNH_2 (sym.)
3	2	3191	w	3198	w			3183	w	3205	3089	7.62	141.33	72.50	96 νCH
4	20b	3073	m	3060	m	3063	w	3066	s	3188	3073	21.07	142.51	74.23	99 νCH
5	7b	3044	m	3047	m	3037	w			3173	3059	7.19	80.98	42.76	100 νCH
6	13			3033	m					3155	3041	11.97	79.93	42.92	100 νCH
7		3006	m	3002	m	3002	w	2999	m	3130	3017	22.05	110.49	60.71	97 νCH_3 (asym.)
8		2959	m	2956	m	2955	w			3062	2952	37.57	60.58	35.45	100 νCH_3 (asym.)
9		2921	m	2908	m	2908	w	2936	m	3004	2896	57.78	160.04	98.78	98 νCH_3 (sym)
10		1625	s	1615	s			1610	s	1654	1623	125.63	42.53	95.84	54 βNH_2 (sciss.); 24 νCC; 17 βCH
11	8b	1619	s							1632	1601	13.22	6.36	14.70	77 βCCC; 17 βNH_2 (rock.)
12	8a							1596	s	1625	1594	9.97	18.45	42.96	51 νCC; 47 βNH_2 (sciss.)
13	19a	1512	vs	1505	s	1506	s	1509	w	1539	1510	147.17	4.37	11.22	47 βCH; 27 βCCC; 16 βCH_3
14		1470	m	1466	s	1468	m			1506	1478	36.00	4.44	11.83	81 βCH_3 (asym.); 15 νCC
15	19b			1460	m	1461	m	1458	m	1491	1463	10.00	3.96	10.76	40 βCH; 28 βCH_3 (sym.); 23 νCC
16						1454	m			1491	1462	8.55	11.10	30.14	98 βCH_3 (asym.)
17				1442	m	1442	m			1475	1447	3.15	2.37	6.57	64 βCH_3 (sym.); 20 βCH
18	3	1332	m	1341	m	1339	w	1340	m	1377	1351	11.29	17.11	53.22	33 βCH; 32 νCC; 24 βNH_2 (rock.)

Table 4.2 Continued.

No[a]		Experimental[b]								Calculated					PED (%)
		IR (gas phase)[c]		IR (liquid film)[d]		IR (in CCl_4)[d]		Raman[e]		Unscaled	Scaled	I_{IR}	S_{IR}	I_{Ra}	
19	14			1303	m	1304	w			1330	1305	10.01	0.60	1.99	60 βCH; 17 νCC; 11 βNH_2 (rock.); 10 βCH_3
20	20a	1274	s	1275	s	1275	s	1278	m	1300	1275	99.86	16.59	56.79	41 βCH; 26 βCCC; 26 νCN; 12 βCH_3 (sym.)
21		1227	vs	1226	s	1225	vs	1224	w	1246	1222	198.01	3.56	13.06	46 $\nu(CO+OCH_3)$; 29 βCH; 24 βCCC
22		1186	m	1182	s	1183	s	1190	w	1204	1181	23.96	5.10	19.76	63 βCH_3 (asym.); 16 βCH; 10 βNH_2 (rock.)
23	9a							1157	m	1182	1160	0.35	6.99	27.85	86 βCH
24		1145	m	1141	m	1142	m			1169	1147	0.63	2.60	10.55	87 βCH_3 (asym.); 10 γCOC
25	7a									1162	1140	22.14	1.51	6.19	54 βCH; 22 βNH_2 (rock.); 14 βCH_3
26		1079	m	1074	m	1072	m			1090	1069	27.89	2.16	9.79	38 βNH_2 (rock.); 33 βCH; 15 νCC; 14 νOCH_3
27	18b	1046	m	1045	s	1048	s	1043	s	1069	1049	34.99	12.67	59.13	51 βCH; 20βCCC; 22 νOCH_3
28	18a			1025	s	1029	s	1031	s	1045	1025	15.40	15.32	74.01	57 βCCC; 25 βNH_2 (twist.); 18 νOCH_3 (sym.)
29	17a	906	w	911	m	906	w			953	935	0.06	0.38	2.09	85 γCH; 14 γCCC
30	5									905	888	4.84	0.08	0.46	79 γCH; 17 γCCC
31	12	835	w	843	m	841	w	840	m	852	836	3.54	5.81	38.08	66 βCCC; 23 γNH_2 (wag.)
32	17b									840	824	0.62	0.58	3.91	69 γCH; 21 γCCC
33	6b							757	vs	768	754	14.60	24.82	188.97	60 βCCC; 27 βOCH_3; 13 βNH_2 (rock.)
34	10a	734	s	742	s					748	733	0.81	0.45	3.55	54 γCH; 36 γCCC
35	4									741	727	92.20	1.19	9.53	79 γCH; 15 γCCC
36	6a	593	w	586	m	586	m	589	m	599	587	4.70	6.87	74.91	59 βCCC; 19 γNH_2 (wag.); 16 βCH_3
37										588	577	147.52	2.11	23.60	48 γNH_2 (wag.); 45 γCCC
38	16b									564	554	112.91	2.27	26.96	52 γCCC; 42 γNH_2 (wag.)

Table 4.2 Continued.

No[a]		Experimental[b]				Calculated					PED (%)
		IR (gas phase)[c]	IR (liquid film)[d]	IR (in CCl_4)[d]	Raman[e]	Unscaled	Scaled	I_{IR}	S_{IR}	I_{Ra}	
39	15				515 m	514	504	3.96	5.13	69.76	38 βCN; 36 βCO; 26 βCCC
40	9b					510	500	5.73	2.16	29.75	44 βCCC; 26 γNH_2 (wag.); 35 βCOC
41	1		450	453 w	457 w	456	448	20.70	0.27	4.33	65 γCCC; 19 γNH_2 (wag.); 10 γCOC
42					347 w	346	340	10.21	1.78	43.63	61 γNH_2 (twist.); 20 γCCC; 17 βCH_3
43						336	330	15.45	1.64	42.21	45 γNH_2 (twist.); 30 γOCH_3 (tors.); 25 γCCC
44	16a				308 w	299	294	7.65	0.62	19.18	48 γCCC; 39 γCOC; 22 γCN
45					242 m	233	229	2.89	0.78	36.07	46 γCH_3 (tors.); 29 γCCC; 19 βCN
46	10b					235	230	4.42	0.92	41.86	48 γCH_3 (tors.); 28 γCCC; 16 γCN
47	11				188 m	173	170	2.88	1.40	107.08	41 γCO; 39 γCCC; 20 γCN
48						80	79	5.02	0.71	215.99	60 γOCH_3; 39 γCCCC (aniline tors.)

[a] The second entry labels the modes according to the Varsanyi's convention.
[b] s, strong; vs, very strong; m, medium; w, weak; vw, very weak; sh, shoulder.
[c] Taken from Ref. [57].
[d] Taken from Ref. [58]. The mixing parts of the IR spectra of *o*-anisidine (in CCl_4) and CCl_4 are not reported.
[e] Taken from Ref. [59].

Table 4.3 Calculated B3LYP/6-311++G** vibrational frequencies (in cm^{-1}), IR intensities, Raman scattering activities, Raman intensities, and normal mode descriptions for Conf2 of *o*-anisidine together with the experimental vibrational spectral characteristics of *o*-anisidine.

No[a]		Experimental[b]								Calculated					PED (%)
		IR (gas phase)[c]		IR (liquid film)[d]		IR (in CCl_4)[d]		Raman[e]		Unscaled	Scaled	I_{IR}	S_{IR}	I_{Ra}	
1		3501	m	3460	s	3787	m			3674	3542	27.41	47.89	15.91	100 νNH_2(asym.)
2		3412	m	3370	s	3396	m	3355	w	3571	3442	23.03	189.71	69.36	100 νNH_2 (sym.)
3	2	3191	w	3198	w			3183	w	3204	3088	7.60	145.26	74.56	88 νCH
4	20b	3073	m	3060	m	3063	w	3066	S	3188	3073	21.21	139.23	72.53	91 νCH
5	7b	3044	m	3047	m	3037	w			3173	3059	7.24	81.11	42.83	91 νCH
6	13			3033	m					3155	3042	11.82	79.19	42.51	92 νCH
7		3006	m	3002	m	3002	w	2999	m	3130	3018	22.12	110.64	60.78	97 νCH_3 (asym.)
8		2959	m	2956	m	2955	w			3062	2952	37.57	60.53	35.43	100 νCH_3 (asym.)
9		2921	m	2908	m	2908	w	2936	m	3004	2896	57.69	159.83	98.67	98 νCH_3 (sym)
10		1625	s	1615	s			1610	s	1654	1623	126.11	42.43	95.59	54 βNH_2 (sciss.); 24 νCC; 18 βCH
11	8b	1619	s							1632	1601	13.10	6.34	14.65	77 βCCC; 17 βNH_2 (rock.)
12	8a							1596	s	1625	1594	9.78	18.57	43.23	51 νCC; 47 βNH_2 (sciss.)
13	19a	1512	vs	1505	s	1506	s	1509	w	1539	1510	147.23	4.39	11.27	47 βCH; 27 βCCC; 16 βCH_3
14		1470	m	1466	s	1468	m			1506	1478	36.12	4.43	11.81	81 βCH_3 (asym.); 15 νCC
15	19b			1460	m	1461	m	1458	m	1491	1463	9.76	2.25	6.10	35 βCH; 38 βCH_3 (sym.); 20 νCC
16						1454	m			1490	1462	8.70	12.84	34.88	71 βCH_3 (asym.); 16 βCH
17				1442	m	1442	m			1474	1446	3.21	2.36	6.54	64 βCH_3 (sym.); 21 βCH
18	3	1332	m	1341	m	1339	w	1340	m	1377	1351	11.39	17.18	53.41	33 βCH; 32 νCC; 23 βNH_2 (rock.)

Table 4.3 Continued.

No[a]		Experimental[b]								Calculated					PED (%)
		IR (gas phase)[c]		IR (liquid film)[d]		IR (in CCl_4)[d]		Raman[e]		Unscaled	Scaled	I_{IR}	S_{IR}	I_{Ra}	
19	14			1303	m	1304	w			1330	1305	10.08	0.62	2.03	60 βCH; 17 νCC; 11 βNH_2 (rock.); 10 βCH_3
20	20a	1274	s	1275	s	1275	s	1278	m	1300	1275	99.45	16.50	56.46	41 βCH; 26 βCCC; 27 νCN; 12 βCH_3 (sym.)
21		1227	vs	1226	s	1225	vs	1224	w	1246	1222	198.32	3.58	13.14	46 $\nu(CO+OCH_3)$; 29 βCH; 24 βCCC
22		1186	m	1182	s	1183	s	1190	w	1203	1180	23.85	5.08	19.69	64 βCH_3 (asym.); 15 βCH; 10 βNH_2 (rock.)
23	9a							1157	m	1182	1160	0.37	7.01	27.93	86 βCH
24		1145	m	1141	m	1142	m			1169	1147	0.74	2.61	10.58	89 βCH_3 (asym.); 10 γCOC
25	7a									1163	1141	22.03	1.54	6.29	54 βCH; 21 βNH_2 (rock.); 14 βCH_3
26		1079	m	1074	m	1072	m			1090	1070	27.85	2.01	9.09	38 βNH_2 (rock.); 32 βCH; 15 νCC; 14 νOCH_3
27	18b	1046	m	1045	s	1048	s	1043	s	1069	1049	34.71	12.78	59.62	51 βCH; 20βCCC; 23 νOCH_3
28	18a			1025	s	1029	s	1031	s	1045	1025	15.84	15.33	74.04	57 βCCC; 25 βNH_2 (twist.); 18 νOCH_3 (sym.)
29	17a	906	w	911	m	906	w			954	936	0.07	0.39	2.17	86 γCH; 14 γCCC
30	5									906	888	4.89	0.08	0.45	79 γCH; 17 γCCC
31	12	835	w	843	m	841	w	840	m	852	836	3.59	5.81	38.01	66 βCCC; 23 γNH_2 (wag.)
32	17b									840	824	0.64	0.54	3.59	69 γCH; 21 γCCC
33	6b							757	vs	768	754	14.69	24.85	189.14	60 βCCC; 26 βOCH_3; 13 βNH_2 (rock.)
34	10a	734	s	742	s					747	733	1.19	0.43	3.38	53 γCH; 36 γCCC
35	4									742	728	91.89	1.24	9.90	80 γCH; 14 γCCC
36	6a	593	w	586	m	586	m	589	m	599	587	5.22	6.90	75.26	60 βCCC; 19 γNH_2 (wag.); 16 βCH_3
37										588	577	152.21	2.18	24.42	48 γNH_2 (wag.); 46 γCCC
38	16b									565	554	107.30	2.13	25.27	51 γCCC; 42 γNH_2 (wag.)

Table 4.3 Continued.

No[a]		Experimental[b]				Calculated					PED (%)
		IR (gas phase)[c]	IR (liquid film)[d]	IR (in CCl_4)[d]	Raman[e]	Unscaled	Scaled	I_{IR}	S_{IR}	I_{Ra}	
39	15				515 m	514	504	4.38	5.17	70.33	38 βCN; 36 βCO; 26 βCCC
40	9b					510	500	5.97	2.14	29.46	43 βCCC; 26 γNH_2 (wag.); 35 βCOC
41	1		450	453 w	457 w	456	448	20.21	0.26	4.18	65 γCCC; 19 γNH_2 (wag.); 10 γCOC
42					347 w	352	346	20.68	1.12	26.85	46 γNH_2 (twist.); 24 γCCC; 27 βCH_3
43						339	333	6.34	2.33	59.14	55 γNH_2 (twist.); 21 γOCH_3 (tors.); 24 γCCC
44	16a				308 w	300	295	6.25	0.59	18.23	46 γCCC; 39 γCOC; 24 γCN
45					242 m	235	230	2.86	0.77	35.26	46 γCH_3 (tors.); 29 γCCC; 19 βCN
46	10b					232	228	4.25	0.89	41.51	48 γCH_3 (tors.); 28 γCCC; 16 γCN
47	11				188 m	173	170	2.74	1.40	106.73	41 γCO; 40 γCCC; 20 γCN
48						80	79	5.00	0.72	215.90	59 γOCH_3; 39 γCCCC (aniline tors.)

[a] The second entry labels the modes according to the Varsanyi's convention.
[b] s, strong; vs, very strong; m, medium; w, weak; vw, very weak; sh, shoulder.
[c] Taken from Ref. [57].
[d] Taken from Ref. [58]. The mixing parts of the IR spectra of *o*-anisidine (in CCl_4) and CCl_4 are not reported.
[e] Taken from Ref. [59].

The 30 benzene-like normal modes of *o*-anisidine are labeled (second entry in Tables 4.2 and 4.3) with the convention of Varsanyi and Szoke for the substituted benzenes, which was adapted from the Wilson notation for benzene [60, 61]. This allows investigating the substitutional effects on the benzene modes. All benzene modes with the frequencies below 1650 cm^{-1} couple significantly with the $–NH_2$ and $–OCH_3$ vibrations. This causes not only significant shifts in the frequencies of some modes but also in their orderings. For example, compared with the vibrational modes of 2MTA that has sulfur in the place of oxygen atom of *o*-anisidine [43], the orderings of modes 8a and 8b, 12 and 17b, 15 and 10b, and 9b and 1 are exchanged while the frequency of mode 6b upshifts significantly. Such shifts are more significant compared with the *p*-methylaniline (pMA) modes [8].

The NH_2 scissoring and rocking frequencies of *o*-anisidine are nearly the same as those observed in pure aniline and substituted anilines like pMA and 2MTA [8, 43]. They are calculated respectively at 1623 and 1069 cm^{-1}, consistent with the experimental data. The strong vibrational band at around 1270 cm^{-1} (calculated at 1275 cm^{-1} for *o*-anisidine) is known as the C-NH_2 stretching band in aniline and related compounds [38, 52] and couples strongly with the ring modes.

The NH_2 wagging (calc. 577 cm^{-1}) and twisting (Ra. 347 cm^{-1}) vibrations are generally weak and thus difficult to locate on the experimental spectra. However, computations show that the frequencies of these vibrations are strongly dependent on the type and conformation of the ring substituents.

The overall intensity patterns of the calculated and experimental spectra are in general quite consistent to each other. However, as a result of the interaction of *o*-anisidine with its environment, the NH and CH stretching bands that lie above 2800 cm^{-1} have intensities larger in the experimental IR spectra recorded as liquid film and in CCl_4 than in the experimental gas phase and calculated IR spectra. For the same reason, the shapes of the bands that couple with NH_2 wagging in the 550-600 cm^{-1} range vary at different experimental conditions.

4.3 UV-VIS ELECTRONIC ABSORPTION SPECTRA

The calculated electronic absorption spectra of *o*-anisidine in both gas phase and in ethanol at the TD-B3LYP/6-311++G** level using the B3LYP/6-311++G** geometries were plotted using the λ vertical excitation wavelengths (nm) and the *f* oscillator strengths (Figure 4.4). The UV-Vis spectral characteristics of Conf1 and Conf2 were calculated to be the same, indicating that the out of the plane direction of the amino group does not affect the electronic absorption spectra of *o*-anisidine.

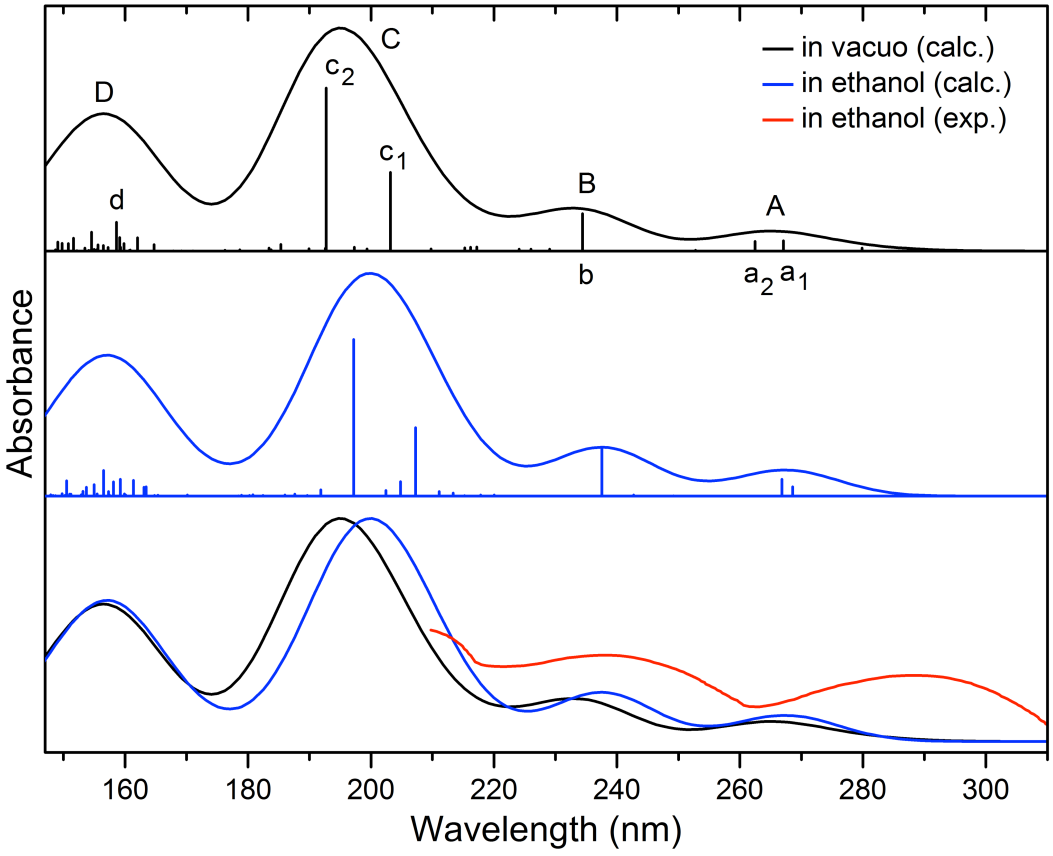

Figure 4.4 Calculated UV-Vis electronic absorption spectra of *o*-anisidine in both gas phase and ethanol, and their comparisons with the experimental spectrum.

The experimental [62] solution-phase UV spectrum of *o*-anisidine recorded in the 210-320 nm range (Figure 4.4) finds two bands at 236 nm (logε = 3.89) and 286 nm (logε = 3.40). These bands were calculated at 238 and 267 nm, respectively. Therefore, while the wavelength of the experimental band at 236 nm was reproduced perfectly, that

of the experimental band at 286 nm is estimated smaller only by around 20 nm. The intensity patterns of these two bands in the calculations and experiment are also consistent to each other. Therefore, the analyses of the electronic absorption spectra of *o*-anisidine at the present computational level are quite promising.

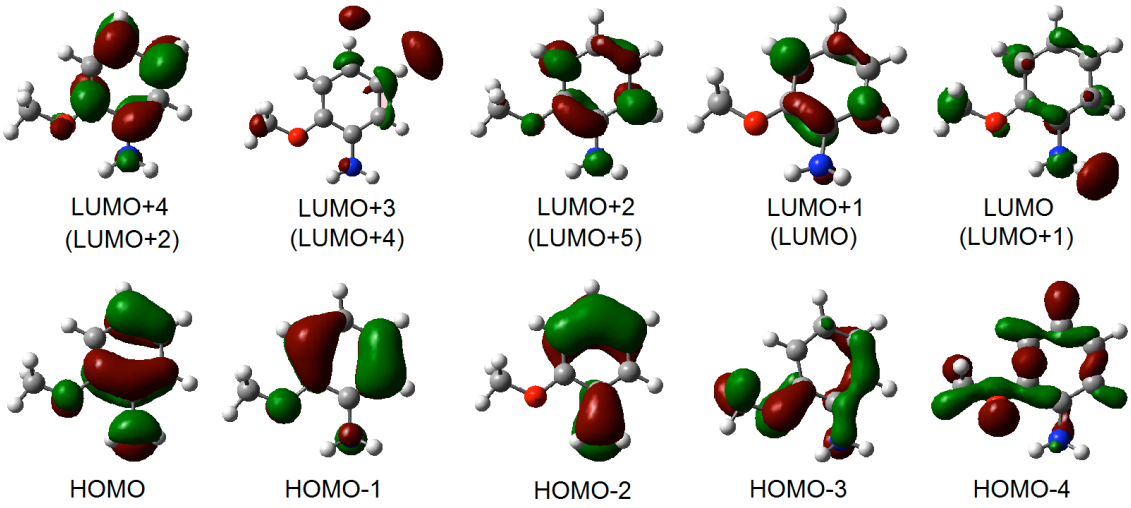

Figure 4.5 Key frontier molecular orbitals of *o*-anisidine in both gas phase and ethanol, labeled out of and in parenthesis, respectively.

The calculations find four absorption bands for *o*-anisidine above 150 nm that are labeled as A, B, C, and D (Figure 4.4). While the bands A and C are due to mainly two transitions (a_1 and a_2 for the band A; c_1 and c_2 for the band C), the bands B and D can be both assigned to a unique transition labeled b and d (Figure 4.4). While the energy ordering of the occupied orbitals of *o*-anisidine in the gas phase [i.e., highest occupied molecular orbital (HOMO) to HOMO-4] is not affected from the introduction of ethanol solution, this causes reordering of the unoccupied orbitals (Figure 4.5). For example, the lowest unoccupied molecular orbital (LUMO), LUMO+1, LUMO+2, LUMO+3, and LUMO+4 in the gas phase structure correspond to LUMO+1, LUMO, LUMO+5, LUMO+4, and LUMO+2 of the structure in ethanol, respectively. The involvement of the unoccupied orbitals in the main transitions of the bands A–D (i.e., a_1, a_2, b, c_1, c_2, and d) varies also going from gas phase to solution structure. Such differences shift all electronic bands slightly to higher wavelengths moving *o*-anisidine from gas phase to ethanol (Figure 4.4 and Table 4.4).

Table 4.4 The λ vertical excitation wavelengths (nm) and *f* oscillator strengths calculated at TD-B3LYP/6-311++G** level for the most intense electronic transitions in each band of the UV-Vis spectrum of *o*-anisidine in both gas phase and ethanol.

Band	Transition	λ (nm)	*f*	Assignment[a,b]
In gas phase				
A	a_1	267	0.03	HOMO → LUMO+1 (82%)
	a_2	262	0.03	HOMO → LUMO+2 (79%)
B	b	234	0.11	HOMO → LUMO+4 (67%)
				HOMO–1 → LUMO+1 (10%)
C	c_1	203	0.24	HOMO–1 → LUMO+2 (29%)
				HOMO–1 → LUMO+1 (18%)
				HOMO–1 → LUMO+4 (15%)
	c_2	193	0.50	HOMO–1 → LUMO+4 (53%)
D	d	155	0.06	HOMO–3 → LUMO+1 (41%)
				HOMO–4 → LUMO+1 (12%)
				HOMO–4 → LUMO (10%)
In ethanol				
A[c]	a_1	269	0.03	HOMO → LUMO+1 (47%)
				HOMO → LUMO (40%)
	a_2	267	0.06	HOMO → LUMO (51%)
				HOMO → LUMO+1 (33%)
B[d]	b	238	0.17	HOMO → LUMO+4 (70%)
				HOMO–1 → LUMO+1 (11%)
C	c_1	207	0.25	HOMO–1 → LUMO+1 (48%)
				HOMO–1 → LUMO+4 (12%)
	c_2	197	0.58	HOMO–1 → LUMO+4 (58%)
				HOMO–1 → LUMO+1 (12%)
D	d	157	0.09	HOMO–3 → LUMO+1 (43%)
				HOMO–4 → LUMO+1 (24%)

[a] The transitions that contribute less than 10% are not shown.

[b] To allow direct comparisons for the orbital types involved in the transitions of gas-phase and ethanol spectra, the orbital labeling of the gas phase structure was used. For example, the LUMO orbital of the gas-phase structure is the LUMO+1 orbital of the structure in ethanol. Instead of LUMO+1 of the structure in ethanol, its relevant orbital in the gas phase structure, i.e., LUMO, was written.

[c] Experimental values: λ_{max} =286 nm; logε = 3.40

[d] Experimental values: λ_{max} = 236 nm; logε = 3.89

We have assigned the main electronic transitions in the UV-Vis spectrum of *o*-anisidine (Table 4.4) in terms of the frontier molecular orbitals (Figure 4.5). The frontier molecular orbital analyses are also useful in estimating several molecular characteristics like chemical reactivity, kinetic stability, and site of electrophilic attack [63, 64]. According to Koopman's theorem [65], the HOMO and LUMO energies are the negative ionization potential *I* and the negative electron affinity *A*, respectively.

$$E_{HOMO} = -I \;\; ; \;\; E_{LUMO} = -A \tag{4.1}$$

The relation of I and A with some other global molecular characteristics like electronegativity χ, chemical hardness η, chemical potential μ, and electrophilicity index ω are as follows [65-69]:

$$\chi = \frac{I + A}{2} \;\; ; \;\; \eta = \frac{I - A}{2} \;\; ; \;\; \mu = -\chi \;\; ; \;\; \omega = \frac{\mu^2}{2\eta} \tag{4.2}$$

Therefore, when the HOMO-LUMO energy gap ΔE is widened, the hardness of the molecule increases while its reactivity decreases [67-70]. The calculated global molecular characteristics of *o*-anisidine obtained using the above relations at the B3LYP/6-311++G** level are given in Table 4.5 for both gas-phase and ethanol structures. These data suggest that *o*-anisidine becomes slightly more stable and slightly less reactive in the solution, owing to its increased ionization potential and reduced electron affinity.

Table 4.5 The calculated global molecular characteristics (eV) of the gas-phase and ethanol structures of *o*-anisidine at the B3LYP/6-311++G** level.

Parameters	In vacuo	In ethanol
E_{HOMO}	-5.44	-5.55
E_{LUMO}	-0.28	-0.22
ΔE	-5.16	-5.33
I	5.44	5.55
A	0.28	0.22
χ	2.86	2.89
η	2.58	2.67
μ	-2.86	-2.89
ω	1.59	1.56

4.4 CHARGE DISTRIBUTION AND MOLECULAR ELECTROSTATIC POTENTIAL ANALYSES

B3LYP charge distribution analyses have been performed by using both the small 6-31G* and the larger 6-311++G** basis sets and by applying Mulliken, electrostatic potential (ESP), and the most sophisticated natural bond orbital (NBO) analyses (Figure 4.6). The average of the already-similar charges on the ring hydrogens (H_{ring}), hydrogens bonded to the nitrogen atom (H_N), and the methyl hydrogens were used in plotting Figure 4.6. Since the charge distribution of Conf1 and Conf2 are found the same, charge analyses in the following are not conformer-specific.

All calculated charges are reasonably close to each other except the Mulliken charges calculated with the larger 6-311++G** basis set for the ring atoms. Mulliken/6-311++G** charges of the ring atoms differ from the other calculated charges not only in the amount significantly but also in the sign. Therefore, one must suspect about the quality of the Mulliken charges when more diffuse and polarization functions are added to the 6-31G* basis set. Actually, the success of the Mulliken scheme with the 6-31G* basis set is not surprising since its parameterization is already based on this basis set [71].

Although ESP charge scheme is more sophisticated than the Mulliken charge scheme, it may also be problematic for electronegative and their neighboring atoms, where the overlap between two orbitals are not partitioned equally [70]. Such kinds of problems in the ESP scheme are not much effective on *o*-anisidine. The most striking difference in the ESP and the most sophisticated NBO charges is the charge of the oxygen atom, being ~0.55*e* in the NBO and Mulliken analyses and ~0.25*e* in the ESP analysis. However, the ESP analysis finds the oxygen atom as one of the most electronegative atom, and is reliable enough for the present case.

The present calculations suggest the most negative atoms as nitrogen and then oxygen. All hydrogen atoms have positive charges; the most is being on the hydrogens bonded to the nitrogen atom. The ring carbons where the substitution occurs have positive charges while the other carbons have negative charges.

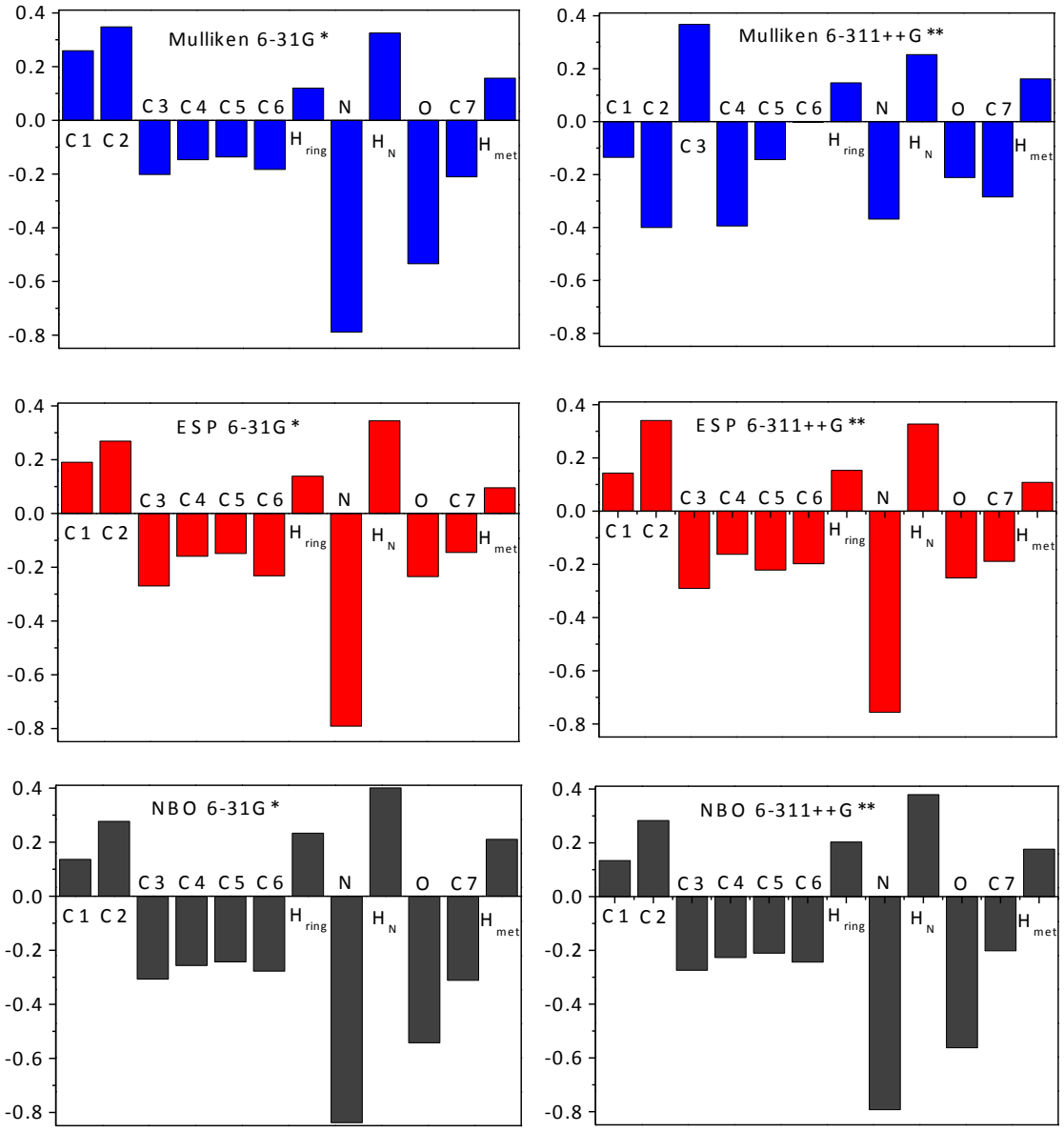

Figure 4.6 B3LYP charges on each atom of *o*-anisidine calculated with the 6-31G* (left) and 6-311++G** (right) basis sets using Mulliken (top), ESP (middle), and NBO (bottom) schemes.

Molecular electrostatic potential (MESP) can be determined experimentally through diffraction methods [71] or be calculated from the electron density obtained from DFT by applying the following formula [72]:

$$V(\vec{r}) = \sum \frac{Z_A}{\vec{R}_A - \vec{r}} \int \frac{\rho(\vec{r}')}{|\vec{r}' - \vec{r}|} d\vec{r}' \tag{4.3}$$

where Z_A is the charge on nucleus A that has the position vector $\vec{R}_A$ and $\rho(\vec{r}')$ is the electron density at the position $\vec{r}'$.

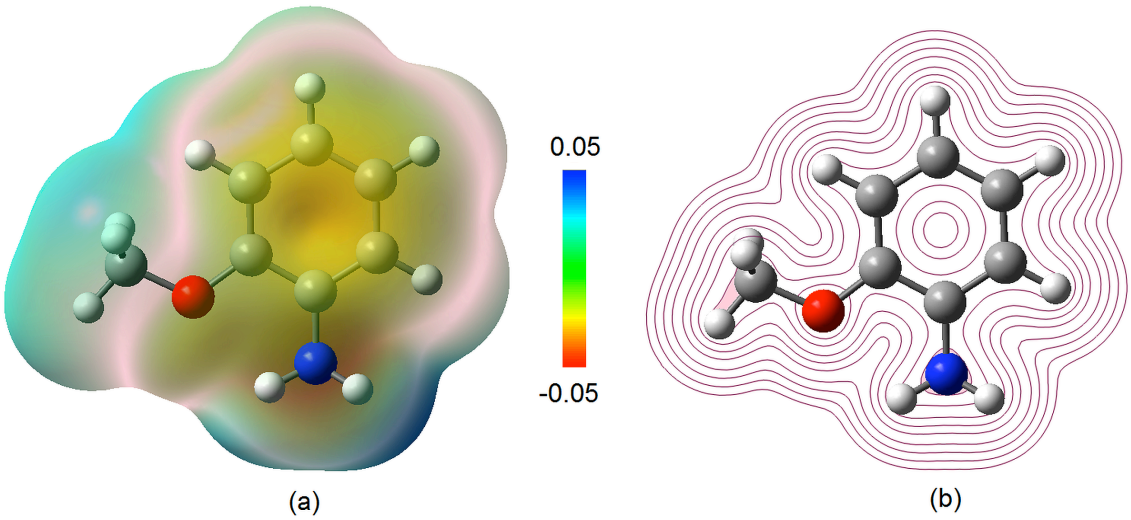

Figure 4.7 (a) The plot of molecular electrostatic potential of *o*-anisidine obtained from the total B3LYP/6-311++G** SCF electron density, and (b) its projection on the ring plane.

The plot of MESP of *o*-anisidine calculated at the B3LYP/6-311++G** is shown in Figure 4.7. In this plot, going from violet to red, electrostatic potential decreases. Therefore, the violet and red regions correspond to positive and negative electrostatic potentials, respectively. The hydrogen atoms reflect positive potential, and thus are the sites of electrophilic attack while the nitrogen and oxygen atoms bear the most electronegative region, and thus have high nucleophilic activity.

4.5 NUCLEAR MAGNETIC RESONANCE SPECTRA

The results of the present GIAO-B3LYP/6-311++G** level chemical shift calculations at both B3LYP/6-31G* and B3LYP/6-311++G** geometries were used in assigning the signals in the experimental [58] ^{13}C and ^{1}H NMR spectra of *o*-anisidine recorded in $CDCl_3$ (Figure 4.8 and Table 4.6) to specific carbons and protons. GIAO-B3LYP/6-311++G** level chemical shift calculations have been already shown to be quite accurate at the B3LYP/6-31G* geometries of several molecules [51-54, 56, 73]. In this study, we also assess the quality of the B3LYP/6-311++G** geometries in reproducing experimental chemical shift values. The chemical shift values of Conf1 and Conf2 have been found to be the same. Therefore, we do not discuss them separately.

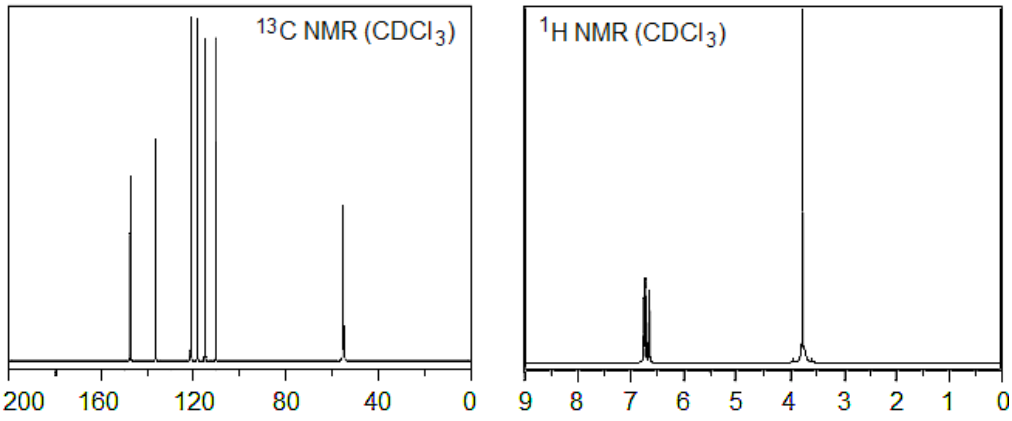

Figure 4.8 Experimental ^{13}C and ^{1}H chemical shifts of *o*-anisidine relative to TMS (in ppm) in $CDCl_3$.

The assignments of the NMR signals of *o*-anisidine are as given in Table 4.6. Although the calculated ^{1}H NMR chemical shifts are very close to the calculated shifts at both geometries, the ^{13}C NMR chemical shifts are overestimated. This arises mainly from the fact that, although the calculations are carried out on single isolated molecules, NMR spectra are quite sensitive to the environment of the molecules, i.e., to the experimental conditions (solvent used or packing in solid state). To relate the experimental and calculated chemical shifts easier, the calculated chemical shifts are

generally scaled [51, 54, 73]. As shown in Figure 4.9, the calculated and experimental chemical shifts correlate very well with R^2 of ~1.0.

Table 4.6 The experimental (in $CDCl_3$) and calculated (unscaled and scaled) ^{13}C and ^{1}H GIAO-B3LYP/6-311++G** chemical shifts of *o*-anisidine relative to TMS (in ppm) at both 6-31G* and 6-311++G** geometries.

Atom	Experiment[a]	6-31G* Geometry		6-311++G** Geometry	
		Unscaled	Scaled	Unscaled	Scaled
C1	136.37	144.40	137.93	143.83	137.78
C2	147.32	154.26	147.07	153.85	147.15
C3	110.55	112.78	108.65	112.87	108.83
C4	118.30	122.78	117.91	122.54	117.87
C5	121.13	126.85	121.68	126.89	121.94
C6	114.99	119.32	114.71	118.83	114.40
C7	55.30	55.95	56.02	56.38	56.01
H3	6.65	6.59	6.54	6.60	6.54
H4	6.70	6.76	6.70	6.76	6.70
H5	6.76	6.92	6.85	6.94	6.87
H6	6.74	6.79	6.73	6.78	6.72
H_{met}	3.77	3.84	3.92	3.87	3.92
H_N	3.70	3.47	3.57	3.51	3.58

[a] Ref. [58].

The correlation equations between the experimental and unscaled chemical shifts δ (in ppm) are as follows

$$\delta_{C,exp}=0.926.\delta_{C,calc}+4.199 \qquad (S = 1.20\ ;\ MAE = 0.81) \qquad (4.4)$$

$$\delta_{H,exp}=0.952.\delta_{H,calc}+0.268 \qquad (S = 0.12\ ;\ MAE = 0.08) \qquad (4.5)$$

at the 6-31G* geometry, and

$$\delta_{C,exp}=0.935.\delta_{C,calc}+3.290 \qquad (S = 1.15\ ;\ MAE = 0.83) \qquad (4.6)$$

$$\delta_{H,exp}=0.960.\delta_{H,calc}+0.206 \qquad (S = 0.13\ ;\ MAE = 0.09) \qquad (4.7)$$

at the 6-311++G** geometry.

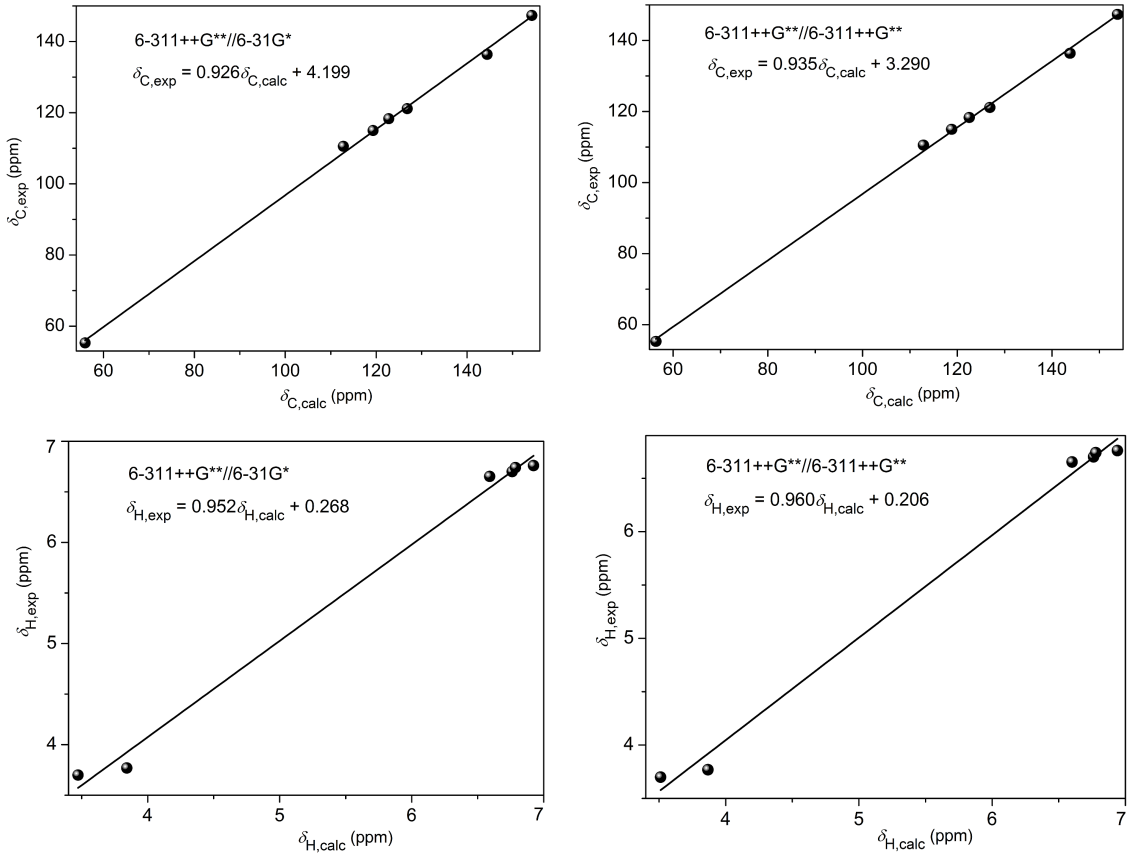

Figure 4.9 Correlation between the experimental and calculated GIAO-B3LYP/6-311++G** level (at both 6-31G* and 6-311++G** geometries) ^{13}C and ^{1}H chemical shifts of *o*-anisidine relative to TMS (in ppm).

The correlation equations and the associated standard errors *S* and the mean absolute errors *MAE* indicate that the calculated chemical shift values at both geometries are quite similar and predictive, with very slight preference to the 6-311++G** and 6-31G* geometries for the ^{13}C and ^{1}H chemical shifts, respectively.

CHAPTER 5

CONCLUSIONS

In this study, the conformational stabilities, geometrical structures, vibrational spectra (both IR and Raman), UV-Vis electronic absorption spectra, the frontier molecular orbitals together with the related global molecular characteristics, molecular electrostatic potential map, and NMR spectra (^{13}C and ^{1}H) of *o*-anisidine have been investigated by using the hybrid B3LYP density functional. All of these molecular features have been calculated using the triple-zeta 6-311++G** basis set. However, the effects of basis set on some of these characteristics have been studied by using the double-zeta 6-31G* basis set, as well.

As a result of the pyramidalized structure of the amino group, the C–N bond in *o*-anisidine is out of the ring plane, which results in two conformations (Conf1 and Conf2). These two conformers have almost the same energy. Thus, *o*-anisidine exists actually as a mixture of these two conformers at the room temperature. All the calculated properties in this study for these two conformers are almost identical. Therefore, their experimental distinction from the recorded spectra seems unlikely. However, the conformers of 2MTA that has sulfur in the place of oxygen of *o*-anisidine were found to have differing spectral characteristics [43]. This difference can be attributed to the fact that the C2–O bond of *o*-anisidine is almost at the ring plane while the C2–S bond of 2MTA is slightly out of the ring plane.

All fundamental vibrational (IR and Raman) bands of *o*-anisidine have been assigned in terms of the present calculations, giving PED of each mode with internal coordinates. The simulated IR and Raman spectra of *o*-anisidine using the scaled

computational wavenumbers, and IR/Raman intensities have been found quite consistent with the experimental spectra.

The calculated TD-B3LYP and experimental electronic absorption spectra of *o*-anisidine agree to each other reasonably. Introducing *o*-anisidine with ethanol affects the energy ordering of the unoccupied orbitals and the involving unoccupied orbitals in the most intense electronic transitions. Such effects shift all electronic bands of *o*-anisidine slightly to longer wavelengths. In the solution, ionization potential of *o*-anisidine increases while its electron affinity decreases. Therefore, solution-phase *o*-anisidine is slightly more stable but less reactive.

In comparison with the results of sophisticated ESP and NBO charges, it has been shown that Mulliken charge analysis is erratic with the 6-311++G** basis set but accurate enough with the smaller 6-31G* basis set, which is already used in parameterization of Mulliken analysis. ESP and NBO charge analyses give similar charges with both basis sets. The most negative atoms of *o*-anisidine are found as nitrogen and then oxygen. All hydrogen atoms have positive charges. The largest positive charges are on the hydrogens bonded to the nitrogen atom. The ring carbons with peripheral substituents have positive charges while the rest of the carbons have all negative charges. The plot of molecular electrostatic potential indicates hydrogens as the sites of electrophilic attack, and N and O to have high nucleophilic activity.

The calculated ^{13}C chemical shifts of *o*-anisidine are slightly larger than the experimental ones. However, the high correlations between the experimental and calculated chemical shifts indicate that the errors in the calculations are systematic and be cured with scaling the chemical shifts. This allowed us certain assignments of the ^{13}C and ^{1}H NMR signals in terms of the present calculations. The calculated B3LYP/6-311++G** chemical shifts at the 6-311++G** and 6-31G* geometries agree very well, with very slight variations. Therefore, both geometries are accurate for calculating NMR properties.

In conclusion, the present structural and spectroscopic calculations have been found quite useful on *o*-anisidine in comparison with the available experiments. Therefore, the computational route followed in this study can be extended in studying molecular characteristics of analogous compounds.

REFERENCES

[1] M. E. Vaschetto, B. A. Retamal and A. P. Monkman, "Density functional studies of aniline and substituted anilines", *Journal of Molecular Structure: Theochem,* vol. 468, pp. 209-221, 1999.

[2] W. B. Tzeng, K. Narayanan, K. C. Shieh and C. C. Tung, "A study of the structures and vibrations of $C_6H_5NH_2$, C_6H_5NHD, $C_6H_5ND_2$, $C_6D_5NH_2$, C_6D_5NHD, and $C_6D_5ND_2$ in the S_1 state by ab initio calculations", *Journal of Molecular Structure: Theochem,* vol. 428, pp. 231-240, 1998.

[3] L. Santos, E. Martínez, B. Ballesteros and J. Sanchez, "Molecular structures and vibrations of m-methylaniline in the S_0 and S_1 states studied by laser induced fluorescence spectroscopy and ab initio calculations", *Spectrochimica Acta Part A: Molecular and Biomolecular Spectroscopy,* vol. 56, pp. 1905-1915, 2000.

[4] J. M. Hermida-Ramón, A. Peña-Gallego, E. Martínez-Núñez, A. Fernández-Ramos and E. M. Cabaleiro-Lago, "A quantum chemical study of aniline/ammonia clusters. Thermodynamic properties and frequency analysis", *Journal of Molecular Structure: Theochem,* vol. 497, pp. 105-113, 2000.

[5] K. Golcuk, A. Altun and M. Kumru, "Thermal studies and vibrational analyses of m-methylaniline complexes of Zn(II), Cd(II) and Hg(II) bromides", *Spectrochimica Acta Part A: Molecular and Biomolecular Spectroscopy,* vol. 59, pp. 1841-1847, 2003.

[6] K. Golcuk, A. Altun and M. Kumru, "Spectroscopic and thermal studies of Mn(II), Co(II) and Ni(II) bromide m-methylaniline complexes", *Journal of Molecular Structure,* vol. 657, pp. 385-393, 2003.

[7] B. Ballesteros and L. Santos, "A reinvestigation of the molecular structures, vibrations and rotation of methyl group in o-methylaniline in S_0 and S_1 states studied by laser induced fluorescence spectroscopy and ab initio calculations", *Spectrochimica Acta Part A: Molecular and Biomolecular Spectroscopy,* vol. 58, pp. 1069-1081, 2002.

[8] A. Altun, K. Gölcük and M. Kumru, "Structure and vibrational spectra of p-methylaniline: Hartree-Fock, MP2 and density functional theory studies", *Journal of Molecular Structure: Theochem,* vol. 637, pp. 155-169, 2003.

[9] A. Altun, K. Gölcük and M. Kumru, "Theoretical and experimental studies of the vibrational spectra of m-methylaniline", *Journal of Molecular Structure: Theochem,* vol. 625, pp. 17-24, 2003.

[10] E. Akalin and S. Akyüz, "Force field and IR intensity calculations of aniline and transition metal(II) aniline complexes", *Journal of Molecular Structure,* vol. 482–483, pp. 175-181, 1999.

[11] M. Stiborová, M. Mikšanová, V. Havlíček, H. H. Schmeiser and E. Frei, "Mechanism of peroxidase-mediated oxidation of carcinogenic o-anisidine and its binding to DNA", *Mutation Research/Fundamental and Molecular Mechanisms of Mutagenesis,* vol. 500, pp. 49-66, 2002.

[12] M. Stiborova, K. Naiman, M. Martinkova, V. Martinek, M. Svobodova, H. H. Schmeiser and E. Frei, "Genotoxic mechanisms for the carcinogenicity of the environmental pollutants and carcinogens o-anisidine and 2-nitroanisole follow from adducts generated by their metabolite N-(2-methoxyphenyl)-hydroxylamine with deoxyguanosine in DNA", *Interdisciplinary Toxicology* vol. 2, pp. 24-7, 2009.

[13] T. Sivaranjini, S. Periandy, M. Govindarajan, M. Karabacak and A. M. Asiri, "Spectroscopic (FT-IR, FT-Raman and NMR) and computational studies on 3-methoxyaniline", *Journal of Molecular Structure,* vol. 1056–1057, pp. 176-188, 2014.

[14] K. Naiman, M. Martínková, H. H. Schmeiser, E. Frei and M. Stiborová, "Human cytochrome-P450 enzymes metabolize N-(2-methoxyphenyl) hydroxylamine, a metabolite of the carcinogens o-anisidine and o-nitroanisole, thereby dictating its genotoxicity", *Mutation Research/Genetic Toxicology and Environmental Mutagenesis,* vol. 726, pp. 160-168, 2011.

[15] T. Ziegler, "Approximate Density Functional Theory as a Practical Tool in Molecular Energetics and Dynamics", *Chemical Reviews,* vol. 95, pp. 651-667, 1991.

[16] Z. Yin, *Microscopic Mechanisms of Magnetism and Superconductivity Studied from First Principle Calculations,* Ph.D. Thesis, California University, 2009.

[17] R. Peköz, *Interactions of lithium-carbon nanosystems: Molecular dynamics simulations and density functional theory calculations,* Ph.D. Thesis, Middle East Technical University, 2008.

[18] Ö. Akyar, *Density functional theory for trapped ultracold fermions,* M.S. Thesis, Middle East Technical University, 2009.

[19] A. Altun, *Benzenamin-3-metil ve benzenamin-4-metil bileşiklerinin iyotlu geçiş elementleri ile yaptıkları komplekslerin karşılaştırmalı titreşim spektroskopisi,* Ph.D. Thesis, Gebze Institute of Technology, 2003.

[20] P. W. Atkins and R. Friedman, *Molecular quantum mechanics,* 5th ed. Oxford: Oxford University Press, 2011.

[21] W. Kohn and L. J. Sham, "Self-Consistent Equations Including Exchange and Correlation Effects", *Physical Review,* vol. 140, 1965.

[22] G. Ildız, *Sülfon ve sülfonamid gruplu moleküllerin konformasyonlarının ve titreşim enerjilerinin kuantum kimyasal yöntemler ile incelenmesi,* Ph.D. Thesis, Istanbul University, 2008.

[23] L. Piela, *Ideas of quantum chemistry*, Amsterdam; London: Elsevier, 2007.

[24] C. N. Banwell, *Fundamentals of molecular spectroscopy,* 3rd ed. London: McGraw-Hill, 1983.

[25] P. Larkin, *Infrared and raman spectroscopy : principles and spectral interpretation*. Amsterdam; Boston: Elsevier, 2011.

[26] T. Bardakcı, *Structural and spectroscopic investigation of some copper(II) compounds,* M.S. Thesis, Fatih University, 2010.

[27] M. Kocademir, *Experimental studies on vibrational spectra of 5, 6, 7, 8-quinolinecarboxaldehyde molecules,* M.S. Thesis, Fatih University, 2013.

[28] S. Yerci, *Spectroscopic characterization of semiconductor nanocrystals,* M.S. Thesis, Middle East Technical University, 2007.

[29] J. M. Hollas, *Modern spectroscopy,* 4th ed. Chichester: Wiley, 2004.

[30] P. S. Sindhu, *Fundamentals of Molecular Spectroscopy*: New Age International, 2006.

[31] M. F. Kaya, *Bazı Pirolidin Türevlerinin Titreşim Spektroskopisi ile Deneysel ve Teorik Olarak İncelenmesi,* M.S. Thesis, Dumlupınar University, 2013.

[32] T. Kalaycı, *Bazı sentetik zeolitlerde adsorbe edilen nitrofenol izomerlerinin titreşim spektroskopisi ve taramalı elektron mikroskopisi ile incelenmesi,* M.S. Thesis, Mehmet Akif Ersoy University, 2011.

[33] M. J. Frisch, G. W. Trucks, H. B. Schlegel, G. E. Scuseria, M. A. Robb, J. R. Cheeseman, J. J. A. Montgomery, T. Vreven, K. N. Kudin, J. C. Burant, J. M. Millam, S. S. Iyengar, J. Tomasi, V. Barone, B. Mennucci, M. Cossi, G. Scalmani, N. Rega, G. A. Petersson, H. Nakatsuji, M. Hada, M. Ehara, K. Toyota, R. Fukuda, J. Hasegawa, M. Ishida, T. Nakajima, Y. Honda, O. Kitao, H. Nakai, M. Klene, X. Li, J. E. Knox, H. P. Hratchian, J. B. Cross, V. Bakken, C. Adamo, J. Jaramillo, R. Gomperts, R. E. Stratmann, O. Yazyev, A. J. Austin, R. Cammi, C. Pomelli, J. W. Ochterski, P. Y. Ayala, K. Morokuma, G. A. Voth, P. Salvador, J. J. Dannenberg, V. G. Zakrzewski, S. Dapprich, A. D. Daniels, M. C. Strain, O. Farkas, D. K. Malick, A. D. Rabuck, K. Raghavachari, J. B. Foresman, J. V. Ortiz, Q. Cui, A. G. Baboul, S. Clifford, J. Cioslowski, B. B. Stefanov, G. Liu, A. Liashenko, P. Piskorz, I. Komaromi, R. L. Martin, D. J. Fox, T. Keith, M. A. Al-Laham, C. Y. Peng, A. Nanayakkara, M. Challacombe, P. M. W. Gill, B. Johnson, W. Chen, M. W. Wong, C. Gonzalez, and J. A. Pople, "Gaussian 03", Revision C.02, Gaussian, Inc., 2004.

[34] A. D. Becke, "Density-functional thermochemistry. III. The role of exact exchange", *J. Chem. Phys.,* vol. 98, pp. 5648-52, 1991.

[35] C. Lee, W. Yang and R. G. Parr, "Development of the Colle-Salvetti correlation-energy formula into a functional of the electron density", *Physical Review B,* vol. 37, pp. 785-789, 1988.

[36] M. J. S. Dewar and C. H. Reynolds, "An improved set of mndo parameters for sulfur", *Journal of Computational Chemistry,* vol. 7, pp. 140-143, 1986.

[37] R. Krishnan, J. S. Binkley, R. Seeger and J. A. Pople, "Self−consistent molecular orbital methods. XX. A basis set for correlated wave functions", *Journal of Chemical Physics,* vol. 72, pp. 650-654, 1980.

[38] K. Raghavachari, J. A. Pople, E. S. Replogle and M. Head-Gordon, "Fifth-Order Møller-Plesset Perturbation Theory: Comparison of Existing Correlation Methods and Implementation of New Methods Correct to Fifth-Order", *Journal of Physical Chemistry,* vol. 94, p. 5579−5586, 1990.

[39] R. Dennington II, T. Keith and J. Millam, *GaussView*, 2007.GaussView, Version 4.1, Semichem, Inc., Shawnee Mission, KS, 2007.

[40] H. F. Hameka and J. O. Jensen, "Theoretical studies of the methyl rotational barrier in toluene", *Journal of Molecular Structure: Theochem,* vol. 362, pp. 325-330, 1996.

[41] A. P. Scott and L. Radom, "Harmonic Vibrational Frequencies: An Evaluation of Hartree−Fock, Møller−Plesset, Quadratic Configuration Interaction, Density Functional Theory, and Semiempirical Scale Factors", *Journal of Physical Chemistry,* vol. 100, pp. 16502-16513, 1996.

[42] V. Küçük, A. Altun and M. Kumru, "Combined experimental and theoretical studies on the vibrational spectra of 2-quinolinecarboxaldehyde", *Spectrochimica Acta Part A: Molecular and Biomolecular Spectroscopy,* vol. 85, pp. 92-98, 2012.

[43] A. Altun and N. M. Aghatabay, "X-ray, vibrational spectra and density functional studies on cynacure", *Vibrational Spectroscopy,* vol. 64, pp. 68-77, 2013.

[44] G. Keresztury, J. Chalmers and P. Griffiths, "Raman Spectroscopy: Theory in Handbook of Vibrational Spectroscopy, vol. 1, John Wiley & Sons", *New York,* p. 71, 2002.

[45] G. Keresztury, S. Holly, G. Besenyei, J. Varga, A. Wang and J. R. Durig, "Vibrational spectra of monothiocarbamates-II. IR and Raman spectra, vibrational assignment, conformational analysis and ab initio calculations of S-methyl-N,N-dimethylthiocarbamate", *Spectrochimica Acta Part A: Molecular Spectroscopy,* vol. 49, pp. 2007-2026, 1993.

[46] V. Krishnakumar, G. Keresztury, T. Sundius and R. Ramasamy, "Simulation of IR and Raman spectra based on scaled DFT force fields: a case study of 2-(methylthio) benzonitrile, with emphasis on band assignment", *Journal of Molecular Structure,* vol. 702, pp. 9-21, 2004.

[47] V. Krishnakumar, G. Keresztury, T. Sundius and S. Seshadri, "Density functional theory study of vibrational spectra and assignment of fundamental vibrational modes of 1-methyl-4-piperidone", *Spectrochimica Acta Part A: Molecular and Biomolecular Spectroscopy,* vol. 68, pp. 845-850, 2007.

[48] V. Krishnakumar, S. Muthunatesan, G. Keresztury and T. Sundius, "Scaled quantum chemical calculations and FTIR, FT-Raman spectral analysis of 3,4-diamino benzophenone", *Spectrochimica Acta Part A: Molecular and Biomolecular Spectroscopy,* vol. 62, pp. 1081-1088, 2005.

[49] P. L. Polavarapu, "Ab initio vibrational Raman and Raman optical activity spectra", *Journal of Physical Chemistry,* vol. 94, pp. 8106-8112, 1990.

[50] J. Tomasi, B. Mennucci and E. Cancès, "The IEF version of the PCM solvation method: an overview of a new method addressed to study molecular solutes at the QM ab initio level", *Journal of Molecular Structure: Theochem,* vol. 464, pp. 211-226, 1999.

[51] A. E. Aliev, D. Courtier-Murias and S. Zhou, "Scaling factors for carbon NMR chemical shifts obtained from DFT B3LYP calculations", *Journal of Molecular Structure: Theochem,* vol. 893, pp. 1-5, 2009.

[52] T. Bally and P. R. Rablen, "Quantum-Chemical Simulation of 1H NMR Spectra. 2. Comparison of DFT-Based Procedures for Computing Proton–Proton Coupling Constants in Organic Molecules", *Journal of Organic Chemistry,* vol. 76, pp. 4818-4830, 2011.

[53] J. R. Cheeseman, G. W. Trucks, T. A. Keith and M. J. Frisch, "A comparison of models for calculating nuclear magnetic resonance shielding tensors", *Journal of Chemical Physics,* vol. 104, pp. 5497-5509, 1996.

[54] R. Jain, T. Bally and P. R. Rablen, "Calculating Accurate Proton Chemical Shifts of Organic Molecules with Density Functional Methods and Modest Basis Sets", *Journal of Organic Chemistry,* vol. 74, pp. 4017-4023, 2009.

[55] M. W. Lodewyk, M. R. Siebert and D. J. Tantillo, "Computational Prediction of 1H and 13C Chemical Shifts: A Useful Tool for Natural Product, Mechanistic, and Synthetic Organic Chemistry", *Chemical Reviews,* vol. 112, pp. 1839-1862, 2012.

[56] P. R. Rablen, S. A. Pearlman and J. Finkbiner, "A Comparison of Density Functional Methods for the Estimation of Proton Chemical Shifts with Chemical Accuracy", *Journal of Physical Chemistry A,* vol. 103, pp. 7357-7363, 1999.

[57] ChemSpider, A chemical structure database owned by the Royal Society of Chemistry, see: http://www.chemspider.com

[58] SDBS, Spectral database for organic compounds organized by National Institute of Advanced Industrial Science and Technology (AIST), Japan, see: http://sdbs.db.aist.go.jp

[59] Sigma-Aldrich Handbook / Catolog, see: http://www.sigmaaldrich.com/catalog

[60] G. Varsányi, *Assignments for vibrational spectra of seven hundred benzene derivatives,* Halsted Press, 1974.

[61] G. Varsanyi and S. Szoke, "Vibrational Spectra of Benzene Derivatives Academic", *New York,* 1969.

[62] National Institute of Standards and Technology (NIST) Standard Reference Database *69: NIST Chemistry WebBook*, see http://webbook.nist.gov/chemistry/

[63] I. Fleming, "Frontier orbitals and organic chemistry reactions", *Frontier Orbital and Organic Chemistry Reactions,* 1976.

[64] S. Muthu, T. Rajamani, M. Karabacak and A. M. Asiri, "Vibrational and UV spectra, first order hyperpolarizability, NBO and HOMO–LUMO analysis of 4-chloro-N-(2-methyl-2,3-dihydroindol-1-yl)-3-sulfamoyl-benzamide", *Spectro-chimica Acta Part A: Molecular and Biomolecular Spectroscopy,* vol. 122, pp. 1-14, 2014.

[65] R. G. Pearson, "Absolute electronegativity and hardness correlated with molecular orbital theory", *Proceedings of the National Academy of Sciences USA,* vol. 83, pp. 8440-8441, 1986.

[66] C. A. Mebi, "DFT study on structure, electronic properties, and reactivity of cis-isomers of [(NC5H4-S) 2Fe (CO) 2]", *Journal of Chemical Sciences,* vol. 123, pp. 727-731, 2011.

[67] R. G. Pearson, "Absolute electronegativity and absolute hardness of Lewis acids and bases", *Journal of the American Chemical Society,* vol. 107, pp. 6801-6806, 1985.

[68] R. G. Pearson, "Ionization potentials and electron affinities in aqueous solution", *Journal of the American Chemical Society,* vol. 108, pp. 6109-6114, 1986.

[69] R. G. Pearson, "Chemical hardness and bond dissociation energies", *Journal of the American Chemical Society,* vol. 110, pp. 7684-7690, 1988.

[70] D. C. Young, "Computational Chemistry: A Practical Guide for Applying Techniques to Real World Problems. 2001".

[71] M. Gholami, B. Talebi and M. Khalili, "A study of solvent effects on the stereoselectivity of Diels–Alder reactions through molecular surface electrostatic potentials", *Tetrahedron Letters,* vol. 44, pp. 7681-7685, 2003.

[72] J. S. Murray and K. Sen, *Molecular electrostatic potentials: concepts and applications,* vol. 3: Elsevier, 1996.

[73] A. Altun and S. Ok, "NMR analyses and diffusion coefficient determination of minor constituents of olive oil: combined experimental and theoretical studies", *Journal of Chemical and Engineering Data,* vol. 57, pp. 2619-2624, 2012.